2004

SCALE MODELING OF ALUMINUM MELTING FURNACE

Sita rama raju S Penmetsa
University of Kentucky, pssitaramaraju@yahoo.com

ABSTRACT OF THESIS

SCALE MODELING OF ALUMINUM MELTING FURNACE

Secondary (recycled) aluminum constitutes around 48% of the total aluminum used in the United States. Secondary aluminum melting is accomplished in large reverberatory furnaces, and improving its energy efficiency has been one of the major interests to aluminum industries. To assist the industries in improving energy efficiency in aluminum melting, an experimental research furnace (ERF), with 907 kg (2000 lbs) capacity, has been built at the Albany Research Center of the U.S. Department of Energy as part of this multi-partner research program. To verify that the experimental results obtained in the ERF furnace are valid for the operation of industrial furnaces, we used scale modeling technology to assist the validation. In this thesis, scaling laws, which are applied to the thermal conduction loss through the model furnace, were developed and the partial modeling relaxation technique was applied to the development of modeling to derive achievable scaling laws. The model experiments were conducted in the model furnace, which was a one-fourth scaled-down version from the ERF furnace (as a prototype), and then compared to the tests in the ERF furnace. The temperature distributions across both the model and prototype were shown to be in good agreement. Confirmation of the scaling laws demonstrated the usefulness of the scale modeling concept and its applicability to analyze complex melting processes in aluminum melting.

Keywords: scale modeling, scaling laws, aluminum melting, reverberatory furnace

Sita rama raju S Penmetsa

Date:11/17/04

SCALE MODELING OF ALUMINUM MELTING FURNACE

By

Sita rama raju S. Penmetsa

Dr. Kozo Saito
(Director of Thesis)

Dr. George Huang
(Director of Graduate Studies)

Date: 11/17/2004

RULES FOR THE USE OF THESIS

Unpublished thesis submitted for the Master's degree and deposited in the University of Kentucky Library are as a rule open for inspection, but are to be used only with due regard to the rights of the authors. Bibliographical references may be noted, but quotations or summaries of parts may be published only with the permission of the author, and with the usual scholarly acknowledgements.

Extensive copying or publication of the thesis in whole or in part also requires the consent of the Dean of the Graduate School of the University of Kentucky.

THESIS

Sita rama raju S Penmetsa

The Graduate School

University of Kentucky

2004

SCALE MODELING OF ALUMINUM MELTING FURNACE

THESIS

A thesis submitted in partial fulfillment of the requirements for the
degree of Master of Science in Mechanical Engineering
in the College of Engineering at the
University of Kentucky

By

Sita rama raju S Penmetsa

Lexington, Kentucky

Director: Dr. Kozo Saito

(TVA Professor of Mechanical Engineering)

Lexington, Kentucky

2004

…… To My Parents

ACKNOWLEDGMENTS

It is a pleasure to express my deep sense of gratitude and appreciation to all the individuals whose insights and guidance have helped me achieve my thesis objective. First and foremost, I would like to thank my Thesis Chair, Dr Kozo Saito for providing me with an excellent opportunity to work under his able guidance. I would also like to thank Dr. Tianxiang Li, who has been guiding me in every aspect of the thesis and helping me improve the work through his insights. I would also like to acknowledge and appreciate the support and insights provided by Dr Paul King of the Albany Research Center of the Department of Energy whose contributions have helped me improve the quality of my thesis.

Further, I wish to thank the members of my thesis evaluation committee, Dr. Abraham Salazar and Dr. Lawrence E. Holloway, for their evaluation.

The most valuable encouragement and support was provided by my family and friends which helped me succeed in this goal.

I would also like to thank Mr. Brett Spychalski of Allied Mineral Products, Ohio, and the people in the machine shop at the Department of Mechanical Engineering, University of Kentucky, for their help in fabricating my experimental setup. Finally, I would like to thank all the members of the Industrial Applications and Engineering Science (IAES) group for their support and advice throughout.

TABLE OF CONTENTS

LIST OF FIGURES

CHAPTER 1
INTRODUCTION

1.1 BACKGROUND

Aluminum is widely used in the U.S. economy, particularly in the transportation, packaging and construction industries. Of the total aluminum used in the U.S., almost 48% is recycled (secondary) aluminum from both new and old aluminum scraps [1]. Most secondary aluminum melting is accomplished in large reverberatory furnaces. With capacities ranging up to 110 metric tons, these furnaces use natural-gas as fuel to melt large volumes of raw aluminum scraps. According to the recently released report "U.S. Energy Requirements for Aluminum Production," secondary aluminum melting processes, in which the melting process is dominated, account for 20% of the total energy consumed in U.S. manufacturing of aluminum, second only to primary (smelting) aluminum melting. Improving energy efficiency in aluminum melting, while maintaining quality and production, is an important priority for the aluminum industry.

Much effort has been made to improve energy efficiency in melting processes - a 10% improvement in energy efficiency has been achieved in the past decade; however, despite the great progress in improving energy efficiency in aluminum melting, current energy efficiency is still low. It is easy to calculate that the energy required to melt one ton of aluminum is about 1140 mJ (assume final temperature of liquid aluminum is 720 °C); yet, current energy consumption in most reverberatory furnaces in the U.S. is 2,888 to 5,775 MJ/ton [2]. Consequently, energy efficiency is less than 30%; that is over 70% of the input energy is lost during the melting process, of which 35% to 50% is lost through flue gases and heat conduction through furnace walls [3]. Clearly, reducing heat losses and improving energy efficiency have become one of the priorities for aluminum industries.

The U.S. Department of Energy (DOE) funded project "Improving Energy Efficiency in Aluminum Melting" has set a goal to improve energy efficiency in aluminum melting by 25%. This project is a joint effort of several aluminum companies, the national laboratories of the U.S. Department of Energy, and the University of Kentucky. As part of an effort to assist industries to reach this goal, on-site measurements were done on different types of furnaces to evaluate

current furnace performance and suggest improvements. An experimental research furnace (ERF) was built at the Albany Research Center of the DOE for this research purpose. This furnace is smaller than the industrial furnace (1/100, about 907 kg capacity). It's difficult to build the furnace larger because of financial considerations. However, aluminum industries doubt whether the results obtained from the relatively small ERF furnace are valid for the large industrial furnaces and, if the results are valid, how the tests data can be applied. Therefore, we proposed to use scale modeling to assist for validation.

1.2 SCALE MODELING

A scale model is an experimental model structured to mirror the relevant physical behavior of original phenomena, or a prototype. It is a valid substitute for systems that, for some reason (i.e., too large, too small, too fast, too slow, too expensive, inaccessible, and unmanageable), cannot be explored on the prototype. The application of scale model experiments is definitely important for aluminum furnaces because the full-scale aluminum melting furnaces are very large, and it is really difficult to do tests on the prototype because of expenses and tight production schedules at each project-participating company. Therefore, we have built a scaled down model furnace in our lab, which is even smaller than the ERF furnace (1/64 in capacity). The purpose of the scale modeling experiments is similar to what has been said by Johnstone and Thring, "commit your blunders on a small scale and make your profits on a large scale" [4], that is, we conduct model experiments and use principles of scale modeling to establish scaling laws applicable to the model experiments and prototype, and validate the results of the ERF furnace (from scale-model point of view, the ERF furnace will be considered the prototype). If the scaling laws are obeyed in the model experiments, the results obtained from model experiments can be validated to the prototype. If it is as successful as we believe, it will eventually dispel the companies' fears that the results on the test furnace are indeed valid to the industrial furnaces.

1.3 THESIS OVERVIEW

The thesis is divided into chapters devoted to each part of the current study. Chapter 2 introduces the concept of scale modeling and explains in detail the various concepts of scale modeling. Chapter 3 deals with the research objectives and the research approach. Chapter 4

deals with the derivation of scaling laws for thermal conduction across the aluminum furnace walls. Chapter 5 deals with the design and construction of the experimental setup. Chapter 6 presents the experimental results and also discusses the importance of the results obtained. Chapter 7 summarizes the research and presents the conclusions of the work done.

CHAPTER 2
REVIEW OF SCALE MODELING

2.1 INTRODUCTION TO SCALE MODELING

Computers are being increasingly used in the present world to verify and validate the theory behind the engineering phenomena. Despite the acceptance of computers to test theory, there is also a strong interest in experimentation to validate the specific computer simulations by physical testing. Scale modeling is one of the widely used tools for physical testing.

Experiments are often planned and profitably executed as scale model experiments; i.e., lengths, times, forces, temperatures, and electric currents if applied, of the original system, or prototype, are scaled such that the resulting system, or scale model, can be studied as a valid substitute for the original. Such experiments accomplish three salutary things: (a) they permit the transformation to manageable proportions of certain features of the original phenomena that are difficult to handle, such as extreme size, very slow flow, vast energy release, and microscopic dimensions; (b) they shorten experimentation by compacting the number of variables; and (c) they provide a great help to basic understanding of real world phenomena and making inductive references. Thus, through "scaling" of all influential quantities, the original phenomenon, or prototype, is transformed into a "scale" model. That is, the phenomenon is transformed into a similar system which preserves the relative values and proportions of the prototype, even though it may require less (more) space, proceed faster (slower), involve smaller (larger) forces, or result in lower (higher) temperatures [5].

Scale model tests help in understanding the design and scientific fundamentals behind engineering or scientific hardware and phenomenon. A good understanding of the phenomenon at hand is required to apply scale modeling techniques.

Figure 2.1 on the following page summarizes the scale modeling concept using a flowchart.

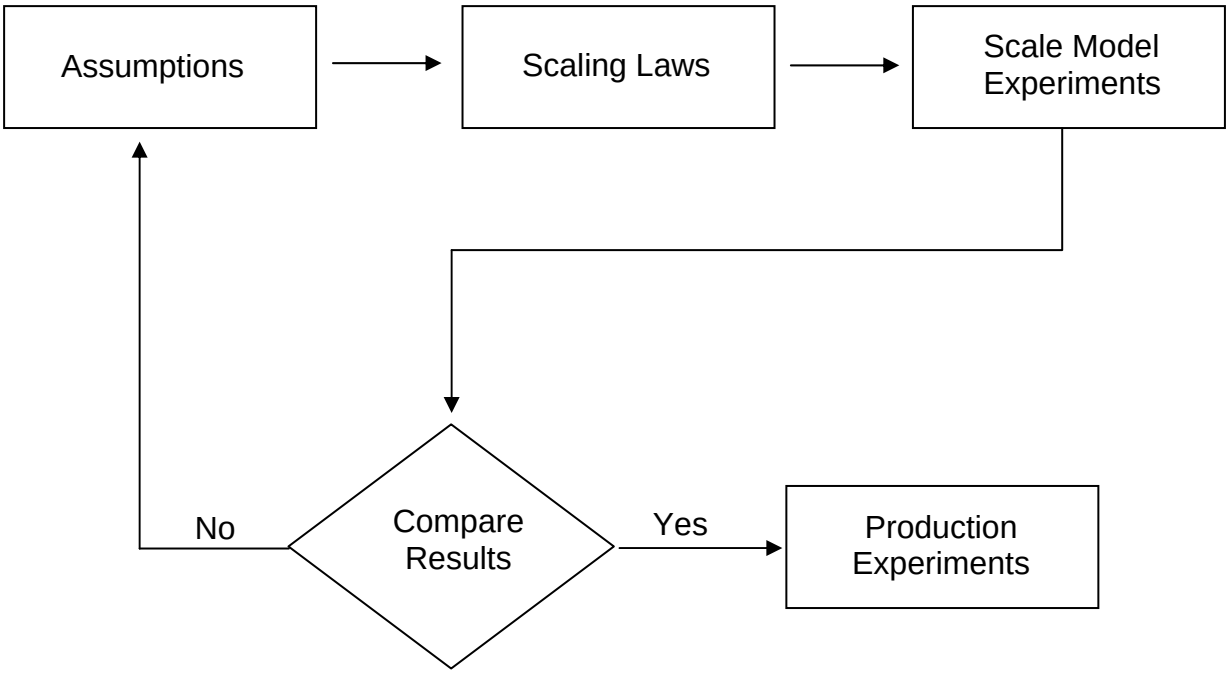

Figure 2.1 Scale Modeling Concept

2.2 PRINCIPLES AND DESIGN OF SCALE MODEL EXPERIMENTS

In scale modeling, research is first done on the prototype elements. We generally account for their physical data of interest; thermal conductivity, heat transfer, geometry, stress, deformation, weight, velocity, acceleration, frequency, magnetic field strength, electric current, etc.

The next stage of research would be looking at ways to get similarity or homologous behavior for the scale model elements. If each quantity of each prototype element can be transformed into the corresponding model elements through multiplication by a respective constant factor or "scale factor," we would be able to obtain a similar scale model.

If l_1, l_2 and l_3 represent the length, width and height of an aluminum prototype furnace, and l_1`, $l_2$`, and l_3` represent the corresponding values of scale model furnace, then homologous furnace geometry requires that

$$\frac{l_1}{l_1'} = \frac{l_2}{l_2'} = \frac{l_3}{l_3'} = l^* \quad \text{..... (2.1)}$$

where l^* is the length scale factor.

Analogous requirements exist for all other corresponding quantities. In general,

$$\frac{q_1}{q_1^{'}} = \frac{q_2}{q_2^{'}} = \frac{q_3}{q_3^{1}} = ... \frac{q_n}{q_n^{'}} = q^* \text{ ..... (2.2)}$$

where q_i and $q_i^{'}$ are the corresponding quantities of the same kind (the primed quantities refer to the model), and q^* is the scale factor. For geometrical similarity, q^* represents the length scale factor; for temporal similarity, the time scale factor; for similarity of forces, the force scale factor; and so forth.

2.2.1 PRIMARY AND SECONDARY QUANTITIES

The next stage in scale modeling is the identification of primary and secondary quantities. Primary quantities are quantities like length, time, temperature etc., and secondary quantities are quantities like area, acceleration etc. which could easily be expressed as a combination of the primary quantities. The exact primary and secondary quantities would depend on the research requirement.

The "primary" scale factors of these primary quantities need to be accounted for, and all the "secondary" scale factors are easily derived from them. For example, consider the primary scale factor of length,

$$\frac{l_1}{l_1^{'}} = \frac{l_2}{l_2^{'}} = \frac{l_3}{l_3^{'}} = l^* \text{ ..... (2.3)}$$

then the area scale factor (secondary scale factor) could be derived as follows,

$$A^* = l^{*2} \text{ ..... (2.4)}$$

Similarly the acceleration scale factor is

$$a^* = l^*/t^{*2} \text{ ..... (2.5)}$$

The secondary scale factor in the present discussion could be expressed as $l^{*n1}\ t^{*n2}\ \theta^{*n3}$ where the exact values n would depend on the secondary quantity considered.

2.2.2 REPRESENTATIVE QUANTITIES AND Pi NUMBERS

If all primary scale factors could be implemented, then all secondary scale factors are automatically satisfied and we have a scale model. To achieve similarity in practical problems, we use the concept of representative quantities and pi-numbers.

The earlier discussed general scaling requirement of

$$\frac{q_1}{q_1^{'}} = \frac{q_2}{q_2^{'}} = \frac{q_3}{q_3^{1}} = ... \frac{q_n}{q_n^{'}} = q^* \quad \text{..... (2.6)}$$

can be contracted to the shorthand notation of

$$q^* = \frac{q_r}{q_r^{'}} \quad \text{..... (2.7)}$$

where q_r and $q_r^{'}$ represent any two corresponding quantities of the same kind. For instance, primary scale length $l^* = l_r / \ l_r^{'}$ indicates that any two corresponding lengths, distances, deformations, or displacements of model and prototype must obey the same length scale factor. Likewise, $\theta^* = \theta_r / \ \theta_r^{'}$ means that any two corresponding wall temperatures, average temperatures, ambient temperatures, temperature differences, etc must follow the same temperature scale factor. The quantities l_r and $l_r`$, $\theta_r$ and $\theta_r`$, are called representative quantities. Expressing in terms of representative quantities,

$a^* = \dfrac{l^*}{t^{*2}}$ can be expressed as $\dfrac{a_r}{a_r^{'}} = \dfrac{l_r}{l_r^{'}} \dfrac{t_r^{'2}}{t_r^2}$

$$\Rightarrow \frac{a_r t_r^2}{l_r} = \frac{a_r^{'} t_r^{'2}}{l_r^{'}} \quad \text{..... (2.8)}$$

Dimensionless products of this kind, composed of representative quantities and required to be equal for model and prototype, are called pi number, since representative nature is understood,

$$\pi = \frac{a_r t_r^2}{l_r} \quad \text{..... (2.9)}$$

A representative quantity in a pi-number can be substituted by any like quantity of the given phenomenon to be modeled. The specific numerical value of a pi-number depends on the numerical values of the quantity we chose to substitute; similarity is only assured if this specific value is maintained for both model and prototype.

2.2.3 MODELING APPROACHES

There are two approaches in development of scaling laws – the equation approach and the law approach. The equation approach uses governing equations to obtain strict scaling laws. In

the equation approach, requirements may be so strict that the scaling laws are sometimes impossible to establish. The law approach may not be so strict, in it some approximations are applied and less important laws are disregarded to enable important scaling laws to be derived. In the law approach, other techniques, such as partial scaling or partial modeling called relaxation, are frequently used to develop scaling laws [6] in which the prototype is divided into several parts according to their phenomena. Different scaling laws are derived for different sections instead of scaling the whole prototype so that model experiments would be much easier. An example of the law approach to derive the Fourier number for an aluminum melting furnace has been discussed in section 2.2.5

2.2.4 PRINCIPAL AND COMMON Pi-NUMBERS

Pi numbers not associated with physical laws are called common pi numbers. An example is the pi number for acceleration derived in section 2.2.3. Pi numbers derived from governing physical laws are called principal pi-numbers. An example of a principal pi-number is the derivation of the Fourier number from two physical laws: Fourier's law of heat conduction, and the law of heat capacity. Fourier's law is usually expresses as

$$q = -k \, grad \, \theta \quad \text{(2.10)}$$

where q is the heat flux (heat energy per unit area and unit time), k is the thermal conductivity, and θ is the temperature. Written in representative terms, Fourier's law takes the form of

$$q \propto k\frac{\theta}{l} \quad \text{(2.11)}$$

The law of heat capacity can be expressed as

$$Q = c_p m \Delta\theta \quad \text{(2.12)}$$

where Q is heat energy, c_p is the specific heat at constant pressure, m is mass, and $\Delta\theta$ is the temperature difference. In representative terms,

$$Q \propto c_p m \theta \quad \text{(2.13)}$$

Expanding Fourier's law of heat conduction yields,

$$q \propto k\frac{\theta}{l} \quad => \quad Q \propto \frac{kl^2\theta}{v} \quad => \quad \pi_k = \frac{Qv}{kl^2\theta} \text{ ..... (2.14)}$$

Similarly expanding the law of heat capacity yields,

$$Q \propto c_p m\theta \quad => \quad Q \propto c_p \rho l^3\theta \quad => \quad \pi_c = \frac{Q}{c_p \rho l^3\theta} \text{ ..... (2.15)}$$

In practical modeling, pi numbers directly derived from physical laws are usually modified by eliminating a representative quantity common to all pi-numbers. By eliminating the representative heat, Q, we arrive at the Fourier number,

$$F_o = \frac{\pi_c}{\pi_k} = \frac{\alpha}{lv} \text{ ..... (2.16)}$$

where $\alpha = k / (\rho Cp)$ is defined as thermal diffusivity.

CHAPTER 3
RESEARCH OBJECTIVE & APPROACH

3.1 BACKGROUND

Primary or secondary aluminum is first melted, alloyed and treated in large gas-fired furnaces, transferred to holding furnaces for additional processing and casted into large D.C. ingots. Although the gas furnaces have different geometries, they all work in a similar manner; heat is transferred to the metal load primarily by heat from the high temperature combustion products and by radiation from the combustion flame, the roof and the sidewalls of the furnace. Aluminum melting is also a source of green house gases (GHG), nitrogen and sulfur oxides. The "Energy and Environmental Profile of the U. S. Aluminum Industry" [2] estimates that emissions from current aluminum melting and casting processes produce ~0.9 lbs/ton of SO_x , ~0.8 lbs/ton of NO_x , and ~430 lbs/ton of CO_2. Clearly, improvements in aluminum melting practices can offer the industry and the nation significant energy savings as well as reduced emissions.

The goal of this jointly funded, multi-partner research program is to improve the energy efficiency of aluminum melting practices by 25%. Full scale implementation of the results of the proposed research by the year 2015 could lead to yearly energy savings of 13 trillion Btu's and related energy cost savings of 57 million dollars per year (using 2000 gas prices) for the U.S. aluminum industry. (13 trillion Btu's is equivalent to energy required to heat 230,000 homes for one year, a small city)

All the industry and research partners in the present project have put their efforts together and have come up with a new furnace design which would help in accomplishing the project goal. A new experimental research furnace of 907 kg capacity has been built at the Albany Research Center, Oregon.

3.2 RESEARCH OBJECTIVE

The capacity of the present furnace is 1/100 of the prototype (industrial aluminum melting furnace). Aluminum industries doubt whether the results obtained from the test furnace are valid for the prototype because of the size, and if the results are valid, how the tests' data could be applied to the prototype. Therefore we proposed to use scale modeling to help the validation.

We have designed and built a small model furnace in our laboratory, which is even smaller than the ERF furnace (1/64 in capacity).We will compare the results of model experiments with the results from the test furnace to examine the availability of scaling laws for aluminum melting furnaces and also to validate the results of the ERF furnace.

3.3 RESEARCH APPROACH

As Hirano and Saito indicated [6] that the key element for scale modeling to be successful is to follow scaling laws. If not, a process that is satisfied in scale model experiments will not guarantee to be satisfied in the prototype, occasionally, reverse results may be found. Therefore, certain scaling laws must be developed in interpreting the results to the full-scale prototype. There are two approaches in developing the scaling laws – the equation approach and the law approach as we mentioned in the previous chapter. The equation approach uses governing equations to obtain strict scaling laws. In the equation approach, requirements may be so strict that the scaling laws are sometimes impossible to establish. The law approach may be not so strict in that some approximations are applied and less important laws are disregarded to enable important scaling laws to be derived. In the law approach, other techniques are used to develop scaling laws. For example, partial scaling or partial modeling is frequently used. This technique is also called relaxation [7] in which the prototype is divided into several parts according to their phenomena. Different scaling laws are applied on each part instead of scaling whole prototype so that model experiments would be much easier. This is the most important technique, and, the process in developing scaling laws may become difficult. Aluminum melting processes are complicated physical and chemical phenomena. Almost all the thermal processes are involved in the aluminum melting, including gas-phase reaction, surface reaction, phase change, heat conduction, heat convection, radiation, mass transfer, and liquid circulation. It is really difficult to design a scale model which includes all these physical and chemical phenomena. Therefore, we will use the partial modeling technique to model aluminum melting processes. Our first step is limited to thermal conduction loss through furnace walls and roof.

CHAPTER 4
SCALING LAWS FOR ALUMINUM FURNACE

4.1 PARTIAL MODELING

In partial modeling, the parameters that significantly influence the physical and chemical phenomena must be selected and grouped based on the scaling laws. These parameter groups, or pi-numbers, are dimensionless and must have the same values in scale model experiments and the prototype (the test furnace). The challenge is to determine how many groups must be selected in order to describe the major physical phenomena existing in the prototype. For heat conduction loss, four thermal processes are essential for describing heat transfer phenomena. These processes are heat generation in combustion space, heat conduction through furnace walls, heat storage within the walls, and natural (or forced) heat convection. Therefore, the corresponding pi-numbers are obtained from these processes. With these considerations, the parameters related to the heat conduction are listed below (for all dimensional symbols, see the nomenclature section) [8]:

length: l, d

physical properties: k, ρ, C_p, h

process parameters: q, t, $\Delta\theta_1$, $\Delta\theta_2$, θ_3

4.2 SCALING LAWS

4.2.1 FIRST SCALING LAW – HEATING SOURCE:

The first scaling law to be considered is the heating source for the model furnace. The important aspect of the heat source associated with the heat conduction is heating intensity rather than heating method, and this gives us flexibility in the model experiments. Besides the length scale, heating intensity and heating time are the parameters that need to be modeled. Thus, the first scaling law is

$$Q_g = ql^3t\,, \tag{4.1a}$$

where Q_g is the total heat generation in the combustion space during the experiment time t. q is the heating intensity (heat generation per unit of volume per unit of time), and l is the

characteristic length of the furnace. The representative form of the heat generation can be written as

$$Q_g \propto ql^3 t\,. \tag{4.1b}$$

Note: The dimensions of the combustion chamber of prototype have been scaled down by one fourth for the model furnace. The scrap inside the furnace has also been scaled down so that the results obtained by scaling down the available heating intensity q inside the furnace are comparable.

4.2.2 SECOND SCALING LAW – HEAT CONDUCTION

The second scaling law to be considered is the heat conduction through the furnace wall. Fourier's Law of heat conduction is given by

$$Q_k = kl^2 \frac{\Delta T_1}{d} t\,, \tag{4.2a}$$

where Q_k is the total heat conducted through a furnace wall during the time t. k is the thermal conductivity of the wall material, ΔT_1 the temperature gradient along the furnace wall, and d the wall thickness. Because the wall thickness in the modeling is also scaled down as the length, the representative form of Fourier's Law yields

$$Q_k \propto kl\theta_1 t\,. \tag{4.2b}$$

where θ_1 is the temperature in representative form for the heat conduction.

4.2.3 THIRD SCALING LAW – HEAT CONVECTION

The heat transferred through heat conduction will be carried away by natural heat convection of ambient air. By definition, the total heat transfer Q_c by natural convection during the time t is

$$Q_c = hl^2 \Delta T_2 t\,, \tag{4.3a}$$

where h is the coefficient of heat transfer by convection, an unknown quantity that must be determined experimentally. ΔT_2 is the temperature difference between the wall surface and ambient air, which is generally of a different order of magnitude with the wall temperature ($\Delta T_2 << \Delta T_1$) so that in representative terms, the heat convection will be the form,

$$Q_c \propto hl^2\theta_2 t\,, \tag{4.3b}$$

4.2.4 FOURTH SCALING LAW – HEAT STORED

In the transient heating process, some heat is stored within the furnace walls. This process can be described by the law of heat capacity,

$$Q_s = \rho dl^2 C_p T_3\,, \tag{4.4a}$$

where Q_s is the total heat stored in the furnace wall, ρ is the density and C_p is the specific heat capacity of the wall material. T_3 is the characteristic temperature of the wall (generally taken an average temperature). Written in representative form, the law of heat capacity is

$$Q_s \propto \rho l^3 C_p \theta_1\,. \tag{4.4b}$$

4.3 Pi NUMBERS

The four scaling laws given above describe the phenomena occurring in heat conduction. Therefore, three principal pi-numbers can be derived based on the law approach.

4.3.1 π_1

The first principal pi-number is the ratio of heat conduction to heat generation, and yields

$$\pi_1 = \frac{Q_k}{Q_g} = \frac{kl\theta_1 t}{ql^3 t} = \frac{k\theta_1}{ql^2}\,. \tag{4.5}$$

π_1 is called the (4th) Damköler number in Schuring's book [5] denoted by $Da_{,IV}$, representing the percentage of heat thermal conduction loss during time t. This heat loss directly affects thermal efficiency of the aluminum furnace so that it is one of the major aspects to be studied in this project.

4.3.2 π_2

The second principal pi-number is taken from the ratio of the heat convection to the heat conduction, which yields

$$\pi_2 = \frac{Q_c}{Q_k} = \frac{hl^2\theta_2 t}{kl\theta_1 t} = \frac{hl\theta_2}{k\theta_1}\,. \tag{4.6}$$

π_2 is known as the Biot number denoted by Bi. It is applied to the heat transfer problem within solid bodies* [5]. Note that the heat loss through furnace walls by heat conduction will be carried away through heat convection at the wall boundaries, so the value of π_2 will be close to unity. In equation 4.6, h is the coefficient of heat transfer by convection which is unknown and must be determined experimentally.

4.3.3 π_3

The third principal pi-number is the derivation of the Fourier number Fo from two physical laws - Fourier's law of heat conduction and the law of heat capacity (heat storage), and can be written as

$$\pi_3 = \frac{Q_k}{Q_s} = \frac{kl\theta_1 t}{\rho l^3 C_p \theta_1} = \frac{kt}{\rho C_p l^2} = \frac{\alpha t}{l^2}. \tag{4.7}$$

where $\alpha = k/(\rho C_p)$ is the thermal diffusivity.

π_3 is a major concern in aluminum melting. This melting occurs mainly through heat transfer from combustion flame to the aluminum loads by heat convection of the flame, and radiation from both flame and furnace walls, in which radiant heat transfer dominates the heating processes. Therefore, the stored heat in the hot walls directly contributes to the radiant heat transfer, thus the aluminum melting rate.

4.4 EXPERIMENTAL RELATIONS

It is convenient to use the same wall materials in the model furnace as the prototype in the model experiments. Therefore, the parameters k, ρ, C_p, α in equations (4.5) - (4.7) are constants. The dimensions of the model furnace (l, d) are scaled down. With these considerations, the three pi-numbers or dimensionless numbers (Da, Bi, Fo) can be simplified to give following relations between the scale model experiments and the prototype,

$$\theta_1 \propto q l^2, \tag{4.8}$$

$$h \propto \frac{\theta_1}{\theta_2 l}, \tag{4.9}$$

* Bi is identical to Nusselt number Nu. Nu is restricted to heat phenomena in a fluid so that k is the thermal conductivity of the fluid. Bi is traditionally applied to heat transfer problem within solid bodies so that k is the thermal conductivity of the body. h is the coefficient of heat transfer by heat convection, which is unknown and must be determined experimentally.

$$t \propto \frac{\theta_1}{q}. \tag{4.10}$$

Equation (4.8) provides the guidance in the model experiments that the selection of heating intensity is flexible, which facilitates the model experiments. The absence of the length scale in equation (4.10) indicates that the ratio of θ_1 and q is independent of the furnace dimensions as long as the same materials are used in model furnace and prototype. Equation (4.9) is used to calculate the coefficient of heat transfer by convection in the model experiments and will be translated to the prototype.

CHAPTER 5
MODEL EXPERIMENTAL CONSIDERATION

5.1 INTRODUCTION

The experimental research furnace (prototype in the present modeling) was built at the Albany Research Center of DOE. The model experimental furnace is designed to mirror the test furnace. It is a rectangular furnace with a door and a chimney installed for further studies of aluminum melting processes. The following table compares the ERF furnace and the model furnace.

Albany furnace particulars:-

- ❖ Combustion chamber dimensions
  - ✓ Length - 1.35 m
  - ✓ Breadth - 1.14 m
  - ✓ Height - 1.01 m
- ❖ Wall Thickness (All faces)
  - ✓ Refractory thickness : 0.14m
  - ✓ Insulation thickness : 0.06m
- ❖ Capacity : 907 Kg Approx (1/100 of industry furnace)
- ❖ Gas fired front charging reverberatory furnace
- ❖ Data acquisition equipment and control with an array of thermocouples (inside and out) on the refractory walls
- ❖ Material details
  - ✓ Side wall and Roof -Hot face : Phlocast 70 AL
  - ✓ Side wall and Roof-Cold face: K-FAC

5.2 FURNACE BUILDING PROCESS AND MATERIAL DETAILS

5.2.1 FURNACE DESIGN

The scale model furnace was designed using AutoCAD (see Figs. 5.1 and 5.2). The furnace dimensions and wall thickness were scaled down to one fourth of the ERF furnace at Albany (as prototype).

The wall materials used are the same as those of the test furnace in hot faces, cold faces and the roof. Each wall has two layers. The hot face was made of AL flow 60, whose maximum service temperature is 1649 °C, much higher than the melting point of aluminum (660°C). The material for the cold face is FBX 1900 Block. Its service temperature limit is 1038°C. Similar materials were used for the roof and the side walls for simplicity. Fireboard HS was used as insulation for the furnace bottom as it has higher compressive strength to support the refractory mass.

The following table summarizes the two furnaces.

PARAMETER	ERF FURNACE	MODEL FURNACE
Combustion Chamber Length	1.35 m	0.34 m
Combustion Chamber Breadth	1.14 m	0.29 m
Combustion Chamber Height	1.01 m	0.25 m
Refractory Thickness	0.14 m	0.03 m
Insulation Thickness	0.06 m	0.01 m
Capacity	907 kg	14.17 kg
Heating Method	Gas Fired	Electrical Heaters
Refractory Material	Phlocast 70 AL	AL Flow 60
Insulation	K- FAC	FBX 1900 Block

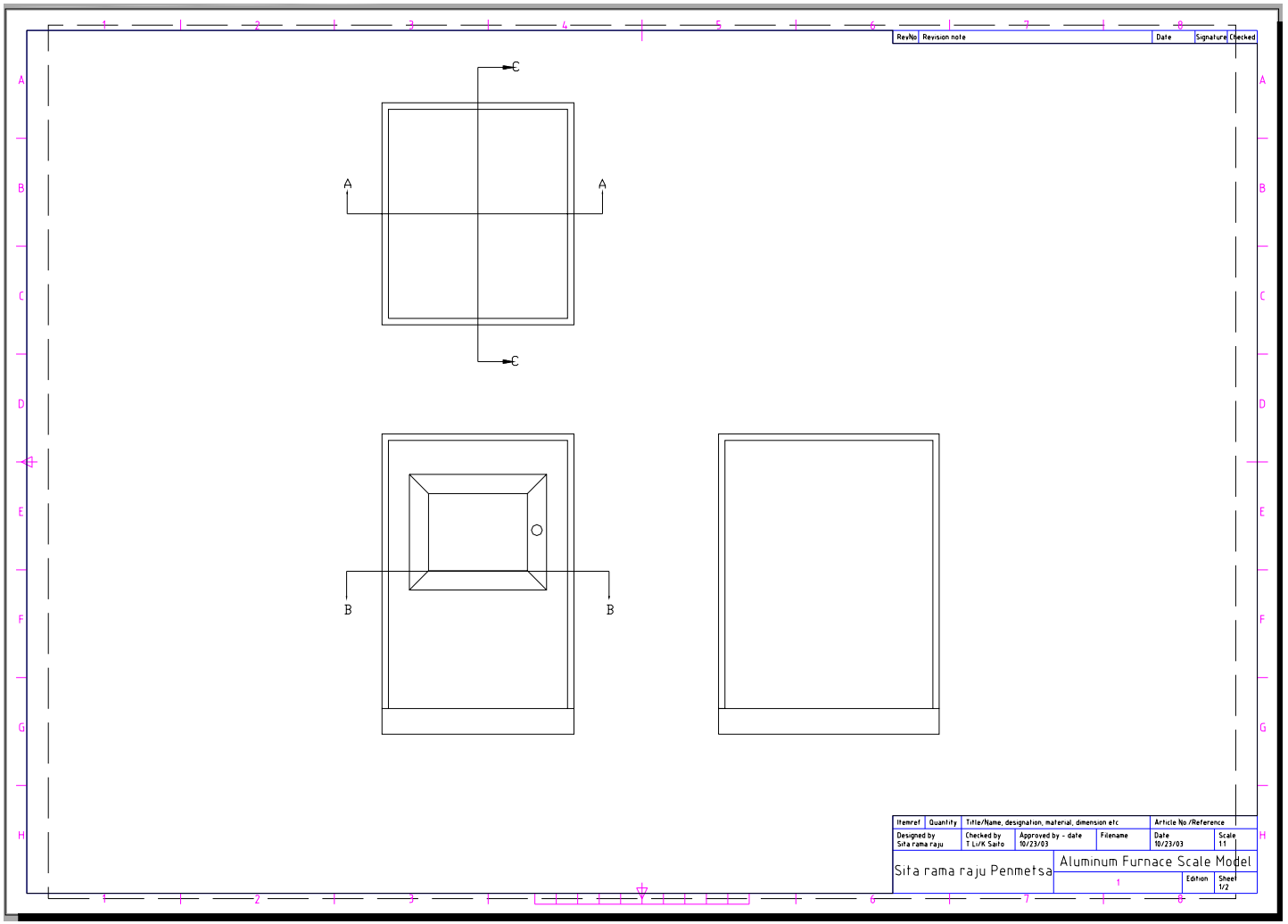

Figure 5.1 Aluminum Furnace Drawing in AutoCAD

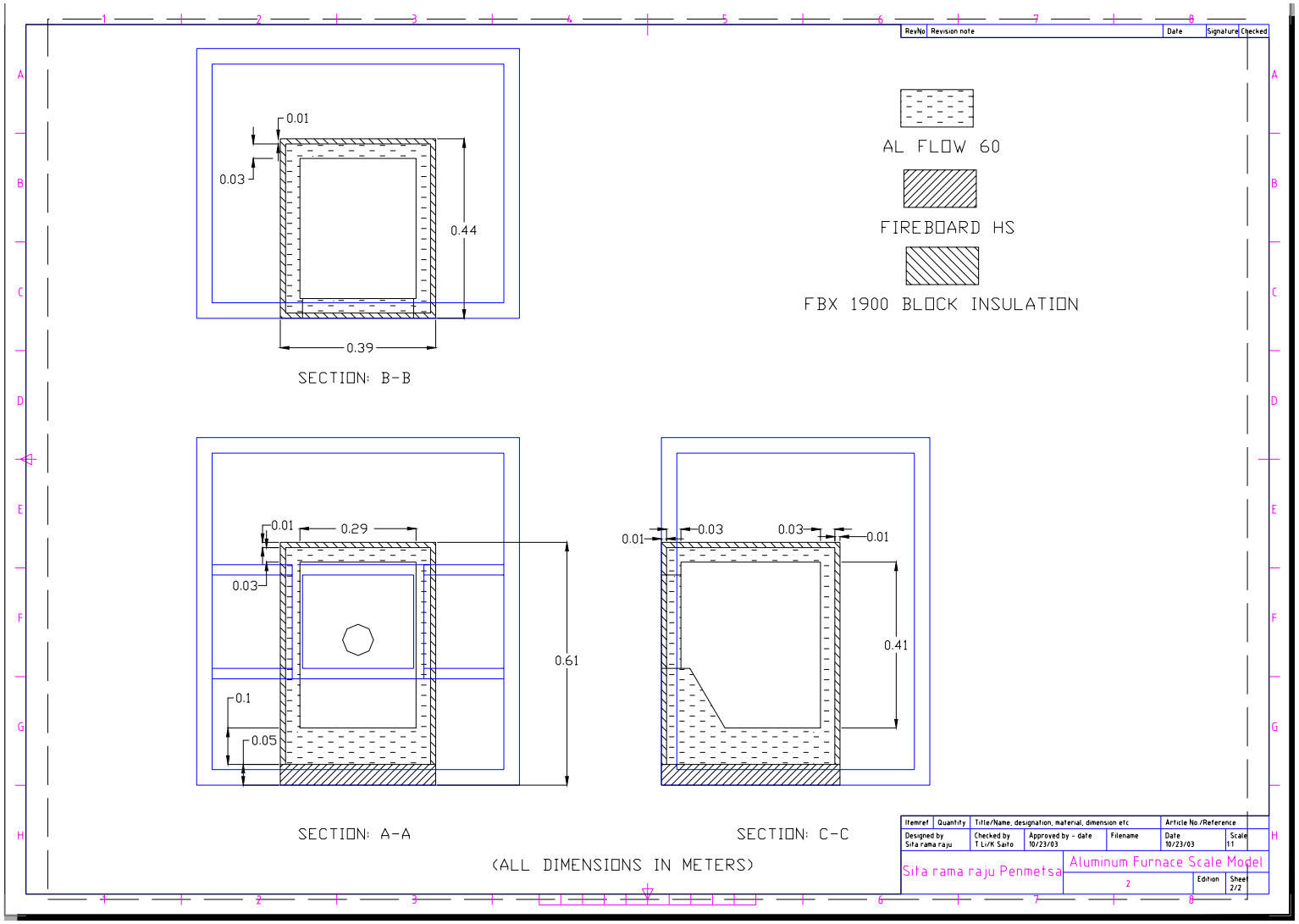

Figure 5.2 Aluminum Furnace Sectional View in AutoCAD

5.2.2 FURNACE FRAME

The first stage in the furnace making was the frame fabrication. The base of the frame was made of half inch thick ASTM A-36 grade hot rolled commercial quality steel plate. The frame was fabricated by welding angular plates whose size is 1-1/2 x 1-1/2 x 1/4 inches. The angular plate material was again ASTM A-36 grade steel. The furnace frame base was mounted on four caster wheels so that the whole experimental setup becomes movable.

Figure 5.3 Scale Model Furnace Frame

5.2.3 FURNACE MOLDS

The second stage in the furnace building process was to make molds. The molds were made of half inch thick commercial plywood. Five different sets of molds were made; the first set was for casting the bottom part which included the base and the bath of the furnace. The second set was for casting the middle part of the furnace which included the exhaust opening and the side walls of the combustion chamber. The third set was for casting the top section of the furnace walls. The fourth set of molds was for casting the roof of the furnace. The fifth set was for casting the refractory of the furnace door.

Figure 5.4 Furnace Molds-Front View

Figure 5.5 Furnace Molds-Side View

After the molds were prepared, the insulation blocks were placed inside the molds in such a way that they would stick to the outer refractory surface of the furnace.

Figure 5.6 Furnace Molds- Top View with Insulation Blocks Inside

The refractory was mixed with water in a commercial mixer and the walls were cast in a sequence starting with the furnace base. The middle section was cast next followed by the top section of the walls. While casting the furnace, the wet refractory was rammed well so that there are no porous refractory portions in the furnace.

Thirteen K-type thermocouples are installed in the model furnace as shown in the figures (5.7) – (5.11) for the measurements of temperature distributions along the wall and surface temperatures inside and outside. Most of these thermocouples have been embedded into the refractory walls and roof during the casting process. Seven thermocouples were placed in the back wall, four of which read the temperature of the inside surface, one reads the temperature at the middle of the refractory cross section, one reads the temperature at the refractory and insulation interface and the seventh one reads the temperature on the back wall surface.

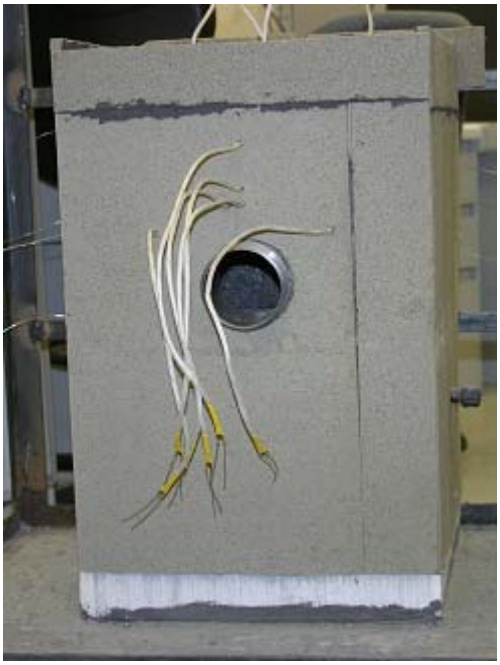

Figure 5.7 Casted Furnace with Thermocouples on the Back Wall

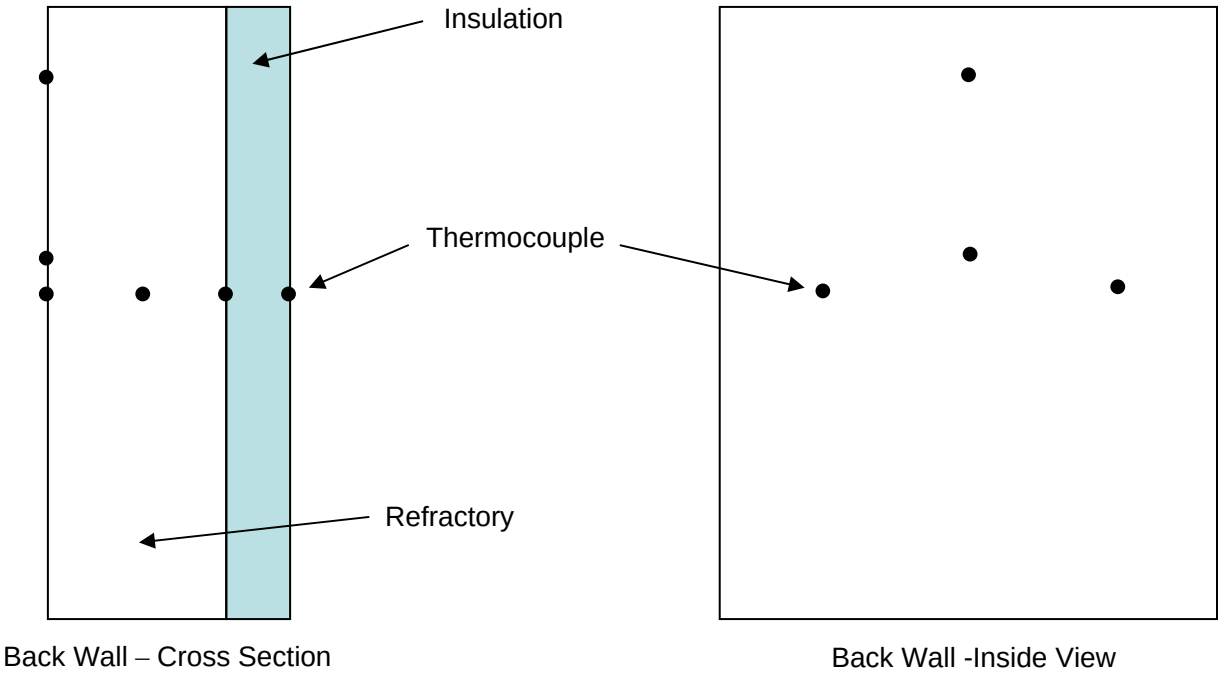

Figure 5.8 Thermocouples arrangement along the Furnace Back Wall

Six thermocouples were embedded in the furnace roof. Three thermocouples would read the inside surface temperature at three different points, one would read the temperature at the interface of insulation and refractory, one would read the roof surface temperature and the sixth one would read the ambient temperature inside the furnace chamber.

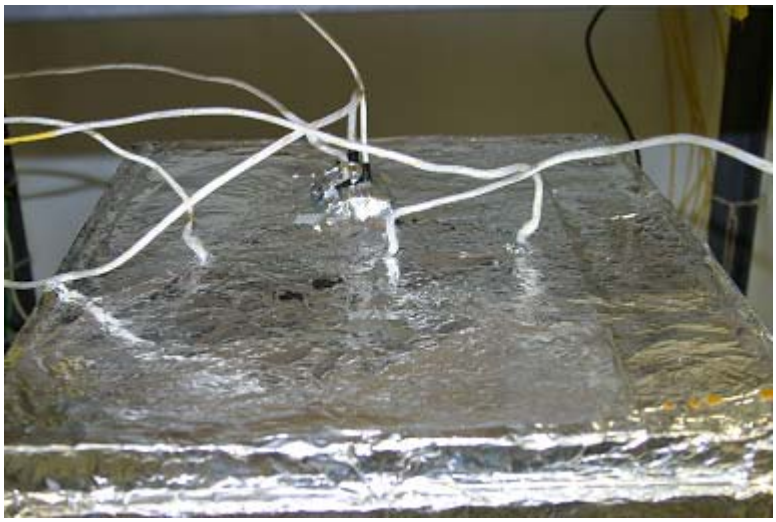

Figure 5.9 Thermocouples on Furnace Roof

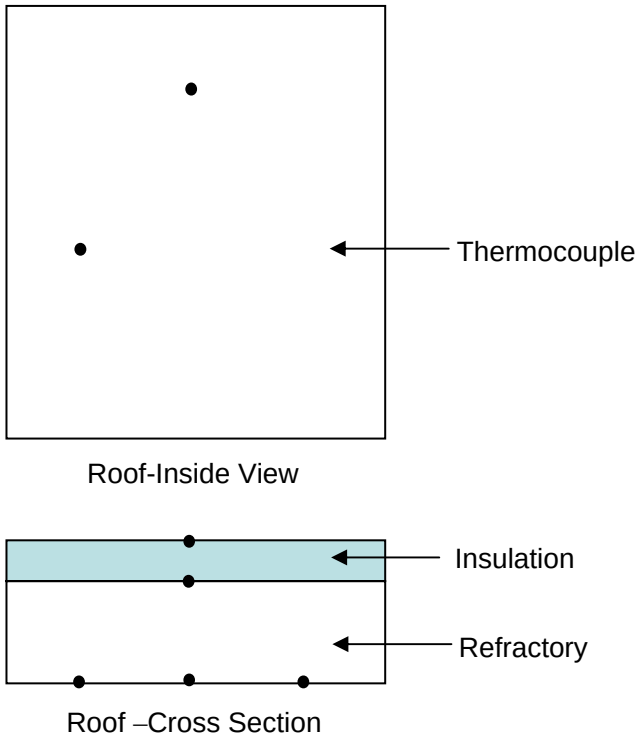

Figure 5.10 Thermocouples arrangement on the Furnace Roof

5.3 FURNACE HEATING MECHANISM

The model furnace uses four 850 W electrical heaters instead of natural gas to supply heat power because the heating method is not essential to the current modeling effort. They were placed on the side walls face to face (see Fig. 5.9).

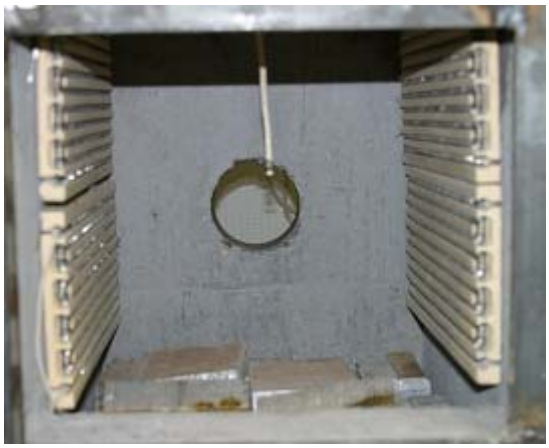

Figure 5.11 Furnace Interior- Electric Heaters, Scrap and Exhaust

The temperature controller provides quick and precise management of temperature inside the furnace. The temperature controller senses the input from one of the K type thermocouples embedded to read the ambient temperature inside the furnace. The output from the temperature controller is connected to solid state relay, which would turn on/off the heaters inside the furnace depending on the temperature settings. The rheostats in the circuit would help in varying the power intensity. This would help in conducting experiments at various heat intensities.

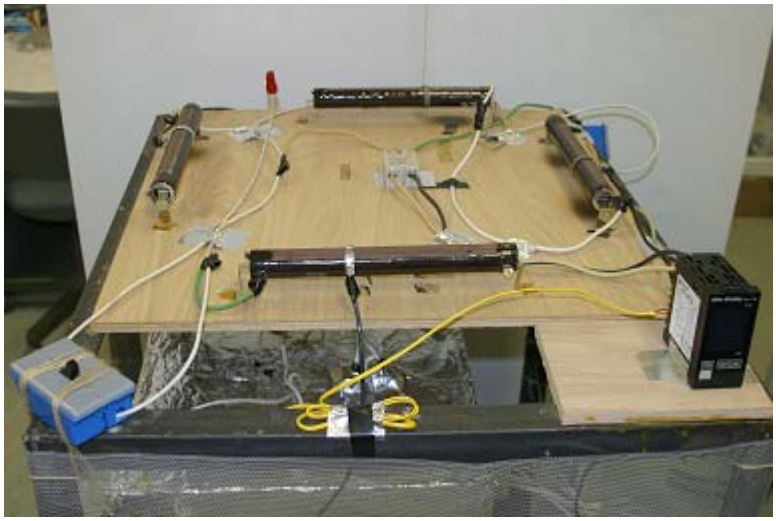

Figure 5.12 Furnace circuit showing various wiring components

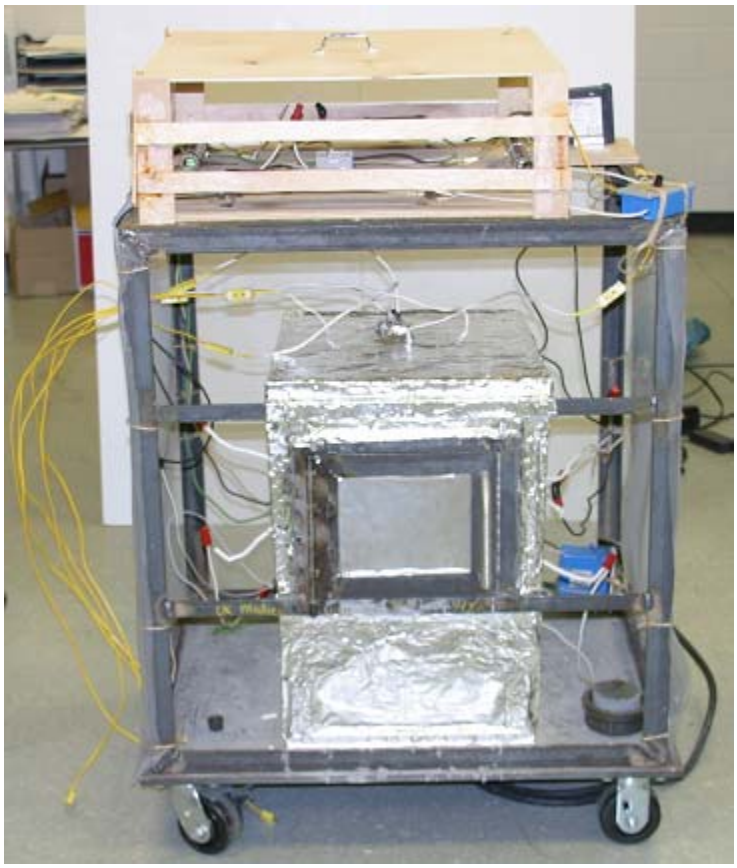

Figure 5.13 Complete Furnace Photograph

5.4 DATA ACQUISITION SYSTEM

Figure 5.14 Data Acquisition Setup

The temperatures will be recorded in a computer-based data acquisition system for analyses. Natural convection will be applied to the cold surface for calculation of *h*. The data will be analyzed and compared with the results obtained from experiments on the test furnace to examine the availability of the scaling laws applicable to aluminum melting processes, which will provide a validation between the results from the test furnace and the prototype.

CHAPTER 6
RESULTS AND DISCUSSION

6.1 INTRODUCTION

The objectives of the research project are to develop the scaling laws for analyzing thermal conduction loss across furnace walls of the aluminum melting furnace, and to verify the applicability of scale modeling applied to the aluminum melting processes. The partial scaling relaxation was applied to the modeling effort. Four scaling laws were developed using the law approach for the analysis of thermal conduction loss across the furnace walls and roof. Three Pi-numbers were created based on the four scaling laws.

The model furnace was built by scaling down the dimensions of the ERF by $1/4^{th}$. The experiments were conducted at various heat intensities by adjusting the heating power of the electric heaters. A data acquisition system was used to record the data and the readings were taken at intervals of fifteen seconds. All the experiments were conducted at nearly the same environmental conditions. The applicability of scaling laws was verified at different heat intensities by comparing the model results with those obtained from the prototype (ERF furnace) for the thermal conduction loss on back walls and roof. In this chapter, the experimental results obtained from the model experiments will be presented, a comparison between the scale model and prototype will be made, and the validation of the scale model to the aluminum melting will be emphasized.

6.2 COMPARISON OF "θ_1/q vs. Time" FOR BACK WALL

Model experiments were conducted for the various heating intensities of q/4, q/5, q/7, q/14, q/16 and q/17, where q is the heating intensity at the ERF furnace (199 kw/m^3). For example, q/4 implies that the heating intensity of the model furnace is 1/4 of the power used in the ERF furnace. The model experiment started at room temperature without forced convection in the room. These experimental conditions are similar to those in the ERF furnace.

Figure 6.1 presents the temporal variation of the ratio of temperature gradient across the back wall, θ_1 to the standard heating intensity, q (heating intensity in the ERF furnace) at the heating intensity of q/4, and compares these data with those measured in the ERF furnace. The experiment was started from room temperature, the ambient temperature of the room being 20^0C

with no forced circulation of air inside the room. These experimental conditions are similar to the conditions under which the prototype experiments were conducted.

Equation (4.10) predicts that the ratio of temperature gradient across the wall and the heat intensity would vary directly with time. This implies that the ratio (θ_1/q) would vary linearly with time under similar experimental conditions.

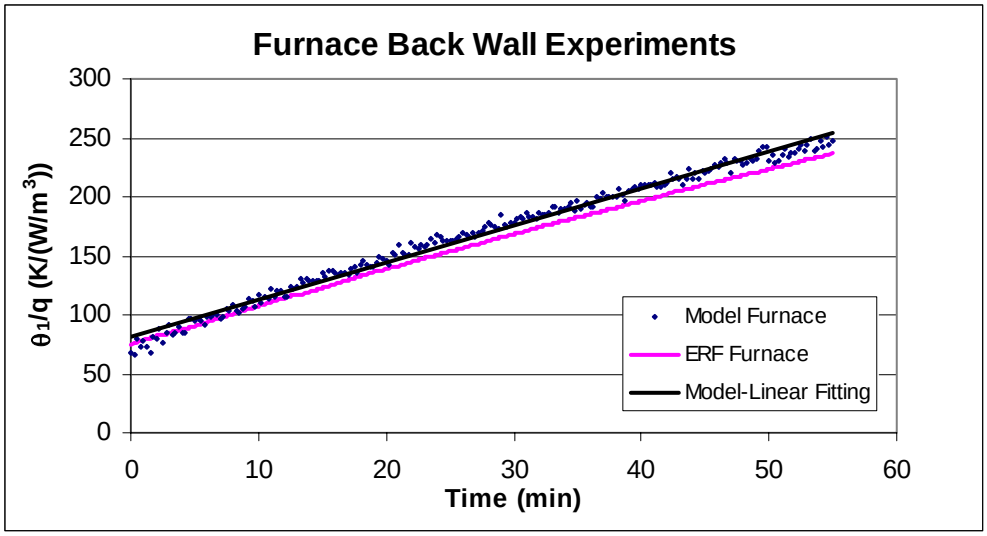

Figure 6.1 Temporal variation of θ_1/q on the back wall of model furnace at q/4 heating intensity and compared with the data from the ERF furnace

Figure 6.1 demonstrates that the results from the model furnace agree well with the prototype furnace (ERF). The important thing to note is the similar slope of the curve for the scale model and prototype. The slight variation is due to rate of heating at the start. In scale model experiments, electric heaters take some time to heat up and start emitting constant heat, whereas in the case of prototype which uses natural gas combustion for heat generation, the heat supply is constant from the start.

The above results confirmed that the ratio of the temperature gradient across the back wall to the heating intensity varies linearly with time in tests on both model furnace and prototype. This ratio is independent of furnace size; therefore, it is expected to be valid in other furnaces without size consideration.

6.2.1 COMPARISON OF "θ_1/q vs. Time" FOR BACK WALL FOR SOME MORE CASES

Figures 6.2-6.6 show the temporal variation of θ_1/q on the back wall at q/5, q/7, q/14, q/16 and q/17 heating intensities. It can be seen that the values of θ_1/q continuously increase with time, and are agreed well with those obtained from the tests in the ERF furnace. At low heating intensities of q/16 and q/17 (Figures 6.6 and 6.7), there was a slight difference in the slope between the data from the model tests and the ERF furnace.

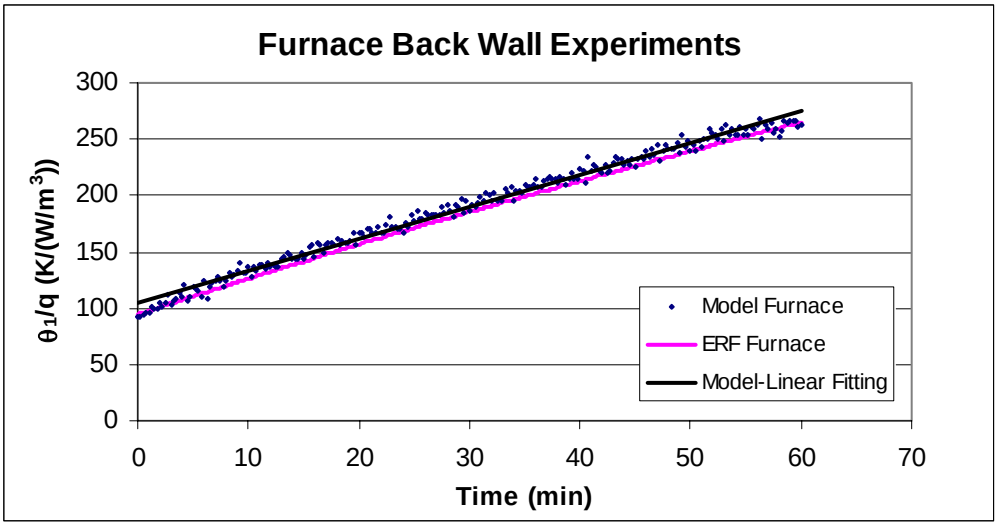

Figure 6.2 Temporal variation of θ_1/q on the back wall of model furnace at q/5 heating intensity and compared with the data from the ERF furnace

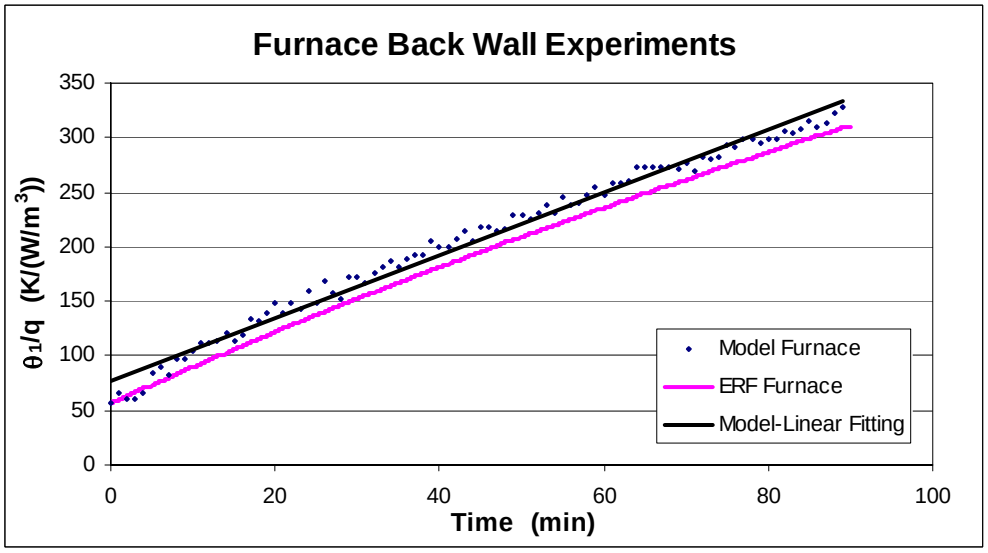

Figure 6.3 Temporal variation of θ_1/q on the back wall of model furnace at q/7 heating intensity and compared with the data from the ERF furnace

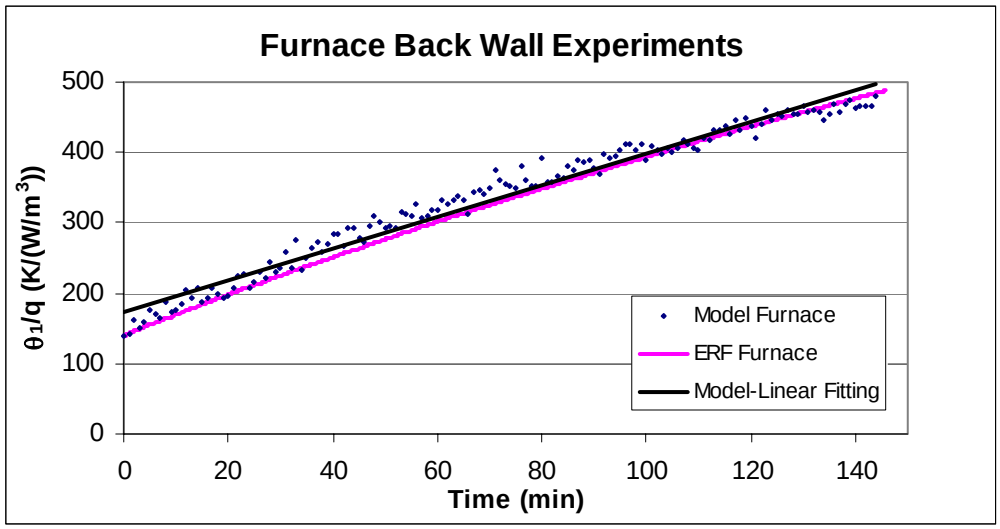

Figure 6.4 Temporal variation of θ_1/q on the back wall of model furnace at q/14 heating intensity and compared with the data from the ERF furnace

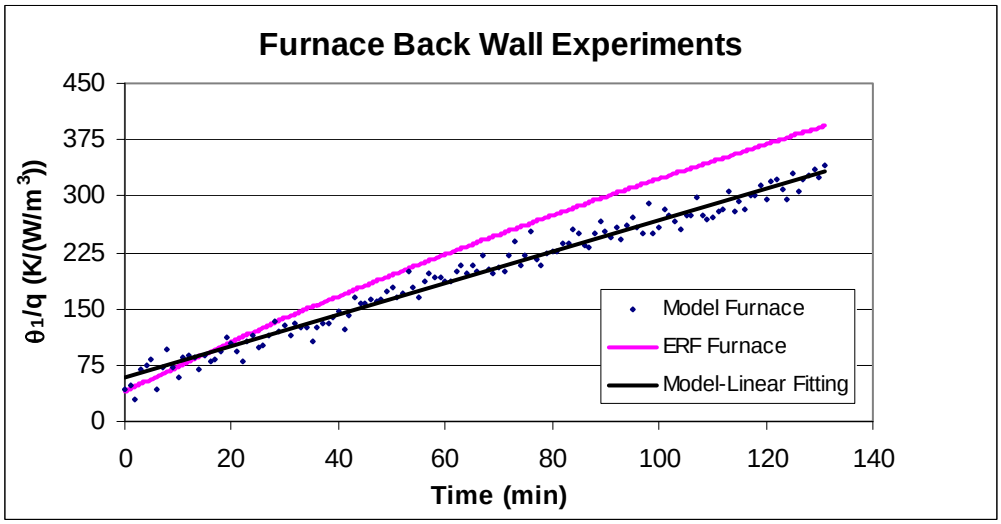

Figure 6.5 Temporal variation of θ_1/q on the back wall of model furnace at q/16 heating intensity and compared with the data from the ERF furnace

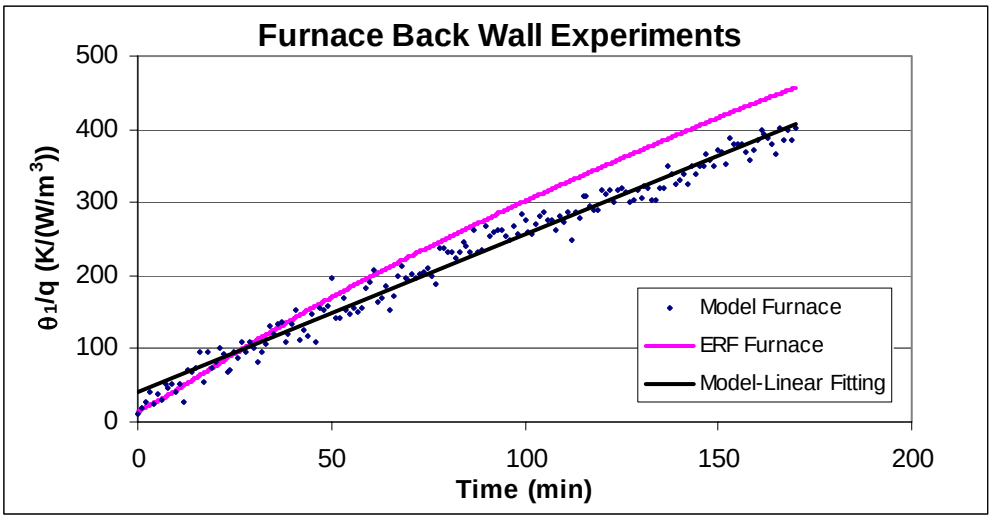

Figure 6.6 Temporal variation of θ_1/q on the back wall of model furnace at q/17 heating intensity and compared with the data from the ERF furnace

The slight variation in slope in case of q/5, q/7 and q/14 is due to the rate of heating at the start. In the scale model, electric heaters take some time to heat up and start emitting constant heat, whereas in the case of prototype which uses natural gas combustion for heat generation, the heat supply is constant from the start. The slight difference in the slope in case of lower heating intensities like q/16and q/17 is due to a mix of very slow rate of heating and the longer experimental time which results in an increase in the heat losses from the furnace because the scale model has very thin walls.

The results shown in Figs. 6.2 - 6.6 confirmed that the ratio of the temperature gradient across the back wall to the heating intensity varies linearly with time in both tests in model furnace and prototype. This ratio is independent of furnace size; therefore, it is expected to be valid in other furnaces without size consideration.

6.3 COMPARISON OF "θ_1/q vs. Time" FOR ROOF

It is known that the thermal conduction loss through furnace roof is much greater than that across furnace walls. As a result the temperature gradient across the roof is not the same as the back wall and this necessitates separate comparison of the scaling laws for the roof.

As shown in figure 6.7, the temperature gradient along the roof of the model furnace was also recorded, and the ratio of this gradient to the corresponding heating intensity is plotted as a function of time. The following graph shows the ratio of temperature gradient across the roof and the heating intensity plotted as a function of time when the model furnace was run with one fourth(49.75 KW/m^3) heating intensity. The experiment was started from room temperature, the ambient temperature of the room being 20^0C with no forced circulation of air inside the room. These experimental conditions are similar to the conditions under which the prototype experiments were conducted.

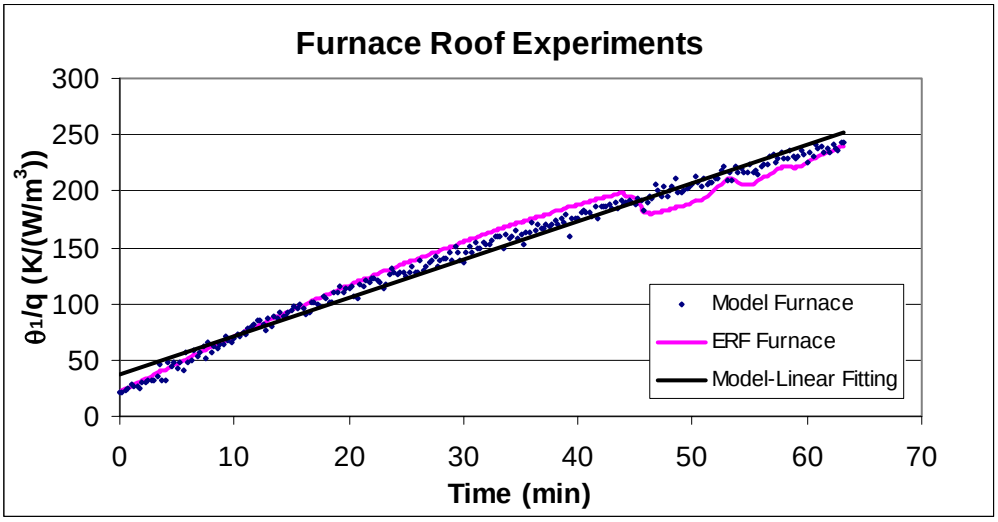

Figure 6.7 Temporal variation of θ_1/q on the roof of model furnace at q/4 heating intensity and compared with the data from the ERF furnace

Figure 6.7 demonstrates that the results from the model furnace agree well with the prototype furnace (ERF). It can be seen that the value of θ_1/q in the model experiments is in good agreement with the ERF data except at around 45 minute's mark where a suddenly reduced θ_1/q occurs in the ERF measurements. This sudden reduction of θ_1/q is believed to be due to door opening for dross removal during the ERF operation. The slight variation is due to a combination of the heating method as well as the rate of heating at the start. In the scale model, electric heaters were used for heat generation whereas in the case of the prototype, natural gas combustion is used for heat generation. As a result there are more gases circulating within the furnace in the case of the prototype, which result in significant heat transfer to the roof by convection, whereas this phenomena is weak in the model furnace. Also electric heaters take

some time to heat up and start emitting constant heat, whereas in the case of the prototype, natural gas combustion is used for heat generation, so the heat supply is constant from the start.

Therefore, the above results prove that the ratio of temperature difference across the furnace roof (θ_1) and the heating intensity varies directly with the heating time. This relationship is independent of the size of the furnace.

6.3.1 COMPARISON OF "θ_1/q vs. Time" FOR ROOF FOR SOME MORE CASES

Roof readings were recorded on all the experiments that were conducted for the back wall, i.e. readings were recorded for experiments conducted for heating intensities of q/4, q/5, q/7, q/14, q/16 and q/17. Here q remains the same, q being the heating intensity of the prototype (ERF) which is 199.0231 KW/m^3. A heating intensity of q/5 implies that the heating intensity is equal to one fifth of that of the prototype, (199.0231/ 5) which would be equal to 39.80 KW/m^3. Similar is the case with other heat intensities.

Figures 6.8 - 6.12 present the experimental results of θ_1/q conducted on the model furnace roof at different heating intensity, q/5, q/7, q/14, q/16, and q/17.

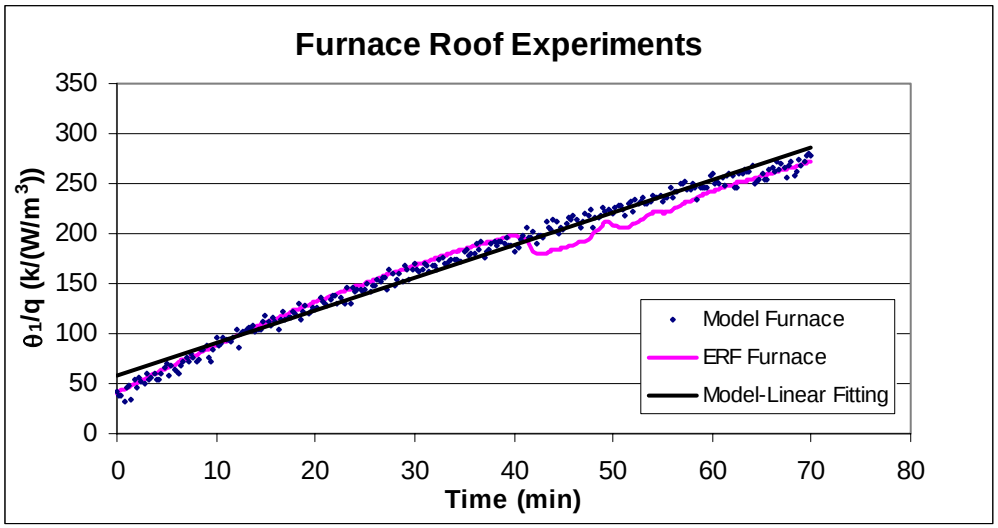

Figure 6.8 Temporal variation of θ_1/q on the roof of model furnace at q/5 heating intensity and compared with the data from the ERF furnace

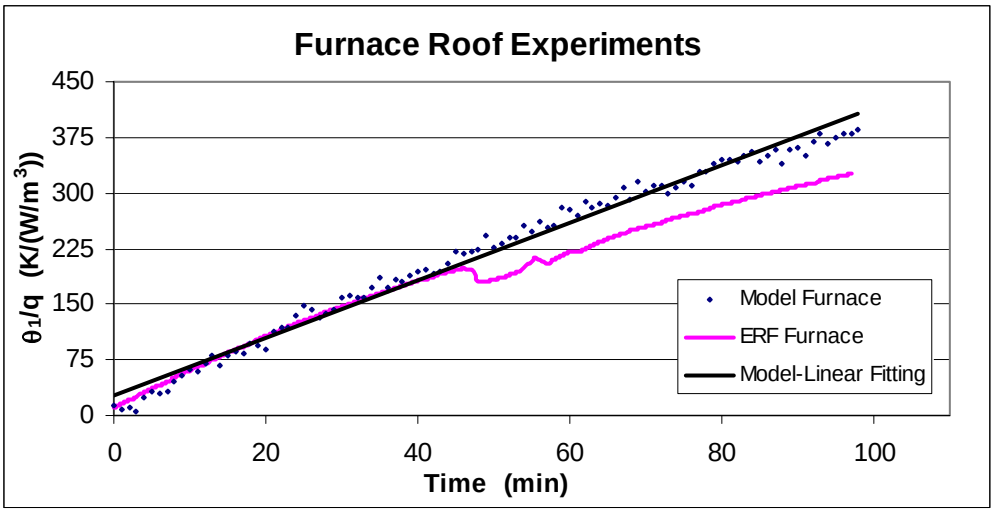

Figure 6.9 Temporal variation of θ_1/q on the roof of model furnace at q/7 heating intensity and compared with the data from the ERF furnace

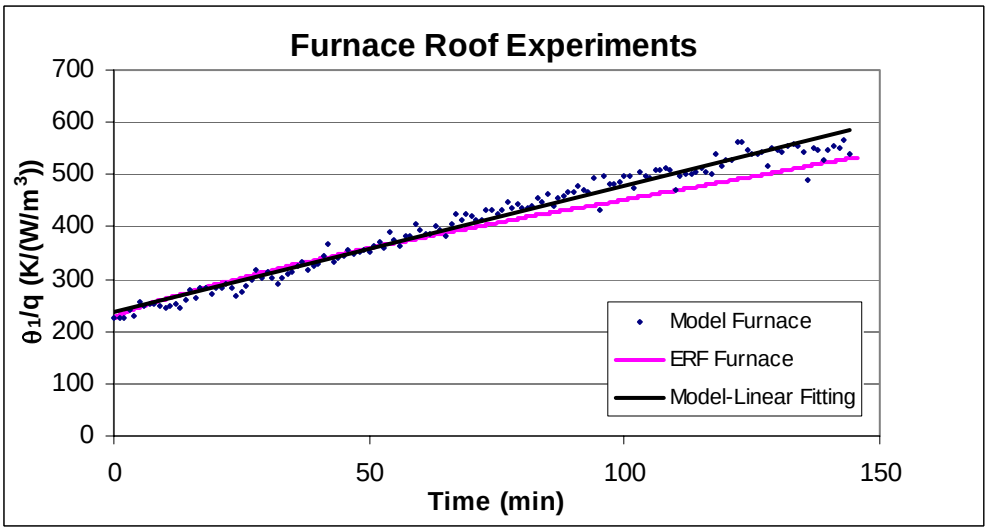

Figure 6.10 Temporal variation of θ_1/q on the roof of model furnace at q/14 heating intensity and compared with the data from the ERF furnace

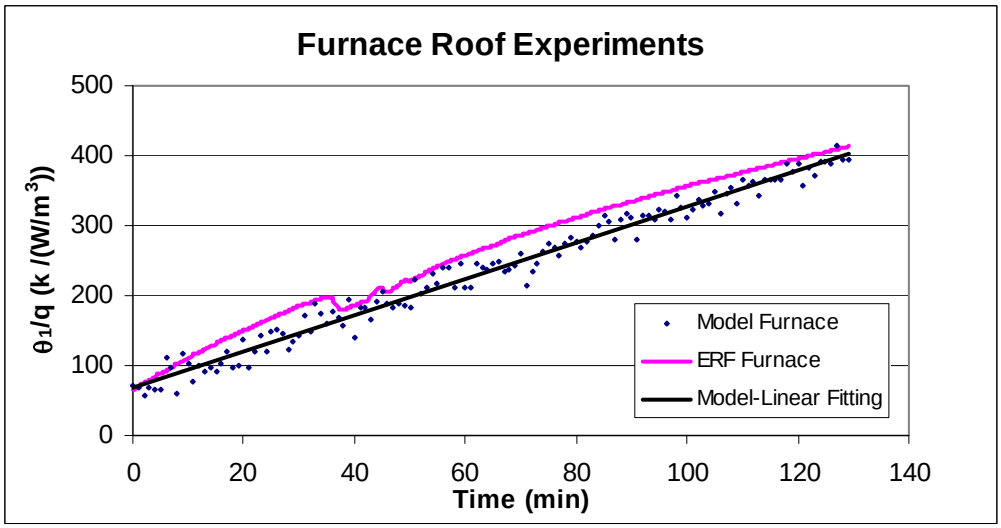

Figure 6.11 Temporal variation of θ_1/q on the roof of model furnace at q/16 heating intensity and compared with the data from the ERF furnace

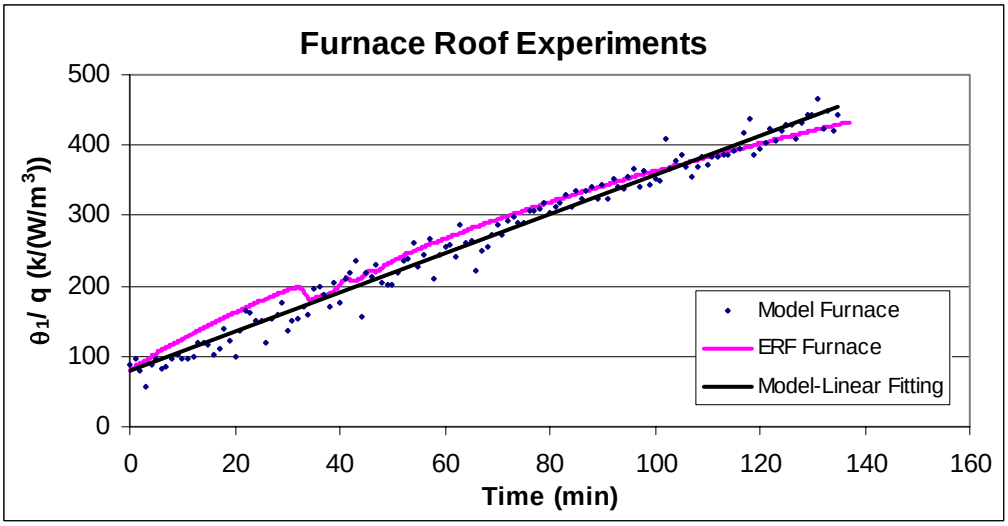

Figure 6.12 Temporal variation of θ_1/q on the roof of model furnace at q/17 heating intensity and compared with the data from the ERF furnace

All these results show a good agreement with those from the tests in the ERF furnace. The slight variation between cases is due to the rate of heating at the start. A slight difference in slope between the tests in the model experiments and in the ERF furnace is due to the rate of change of heating power at beginning of the tests in the model experiments as stated before. Good agreements between the tests in the model experiments and in the ERF furnace on back wall and roof confirmed that the group value of θ_1/q is independent of the furnace dimensions as

indicated in equation 4.10. It is a nature of the furnace performance, so that the test results performed in one furnace may be applied to the others without size consideration for this group value.

6.4 COMPARISON OF "θ1/θ" FOR BACK WALL

The experimental data measured for the back wall could be used to plot a dimensionless term (θ_1/θ), where θ_1 is the temperature across the wall and θ is the initial temperature difference between inside hot face and outside cold face. Dimensionless engineering terms are a convenient help in comparing data obtained from different systems. The assumed relationship ($\theta_1/\theta \ \alpha \ t$) predicts that the ratio of the temperature difference across the wall (θ_1) and the initial temperature difference across the wall (θ) varies directly with time of heating (t). The reason behind making this plot is as follows. Industrial furnaces are rarely started from cold except for newly lined furnaces. They operate continuously and it is valuable to know their behavior as they are continuously fired.

Figure 6.13 plots the temporal variation of θ_1/θ for the back wall with the heating intensity at q/4, and compared with that in the ERF furnace. It shows a good agreement in slope between these two tests in the different furnaces. The good agreement between the model experiments and the ERF tests implies that the dimensionless group θ_1/θ is also an independent variable in the scale model and is not connected with the furnace size.

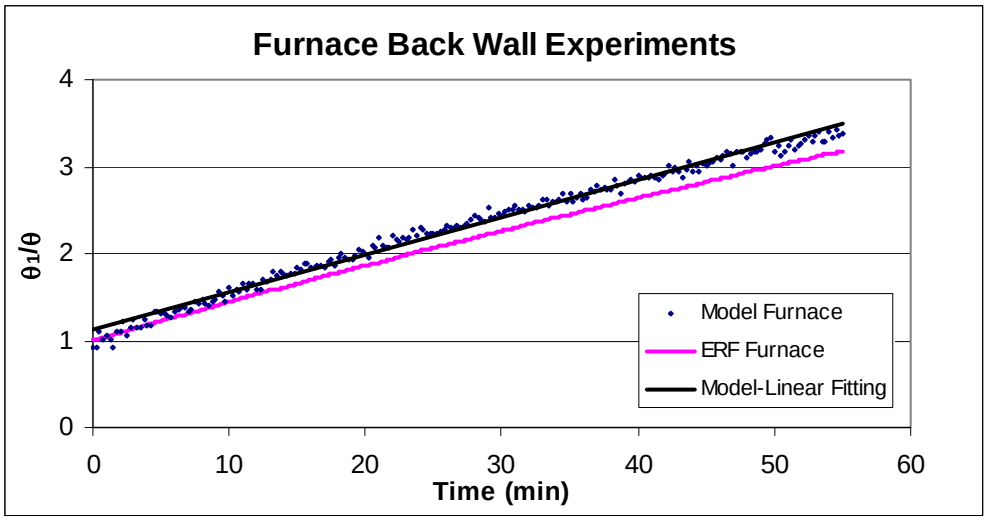

Figure 6.13 Temporal variation of θ_1/θ on the back wall of model furnace at q/4 heating intensity and compared with the data from the ERF furnace.

6.4.1 COMPARISON OF "θ_1/θ vs. Time" FOR BACK WALL FOR SOME MORE CASES

More tests of the group value of θ_1/θ conducted on the back wall are shown in Figures 6.14 - 6.18

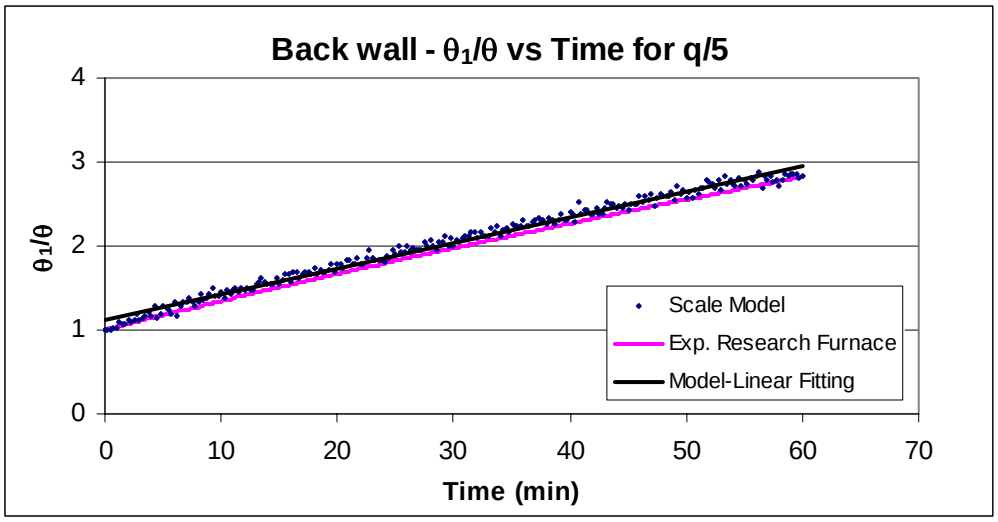

Figure 6.14 Temporal variation of θ_1/θ on the back wall of model furnace at q/5 heating intensity and compared with the data from the ERF furnace.

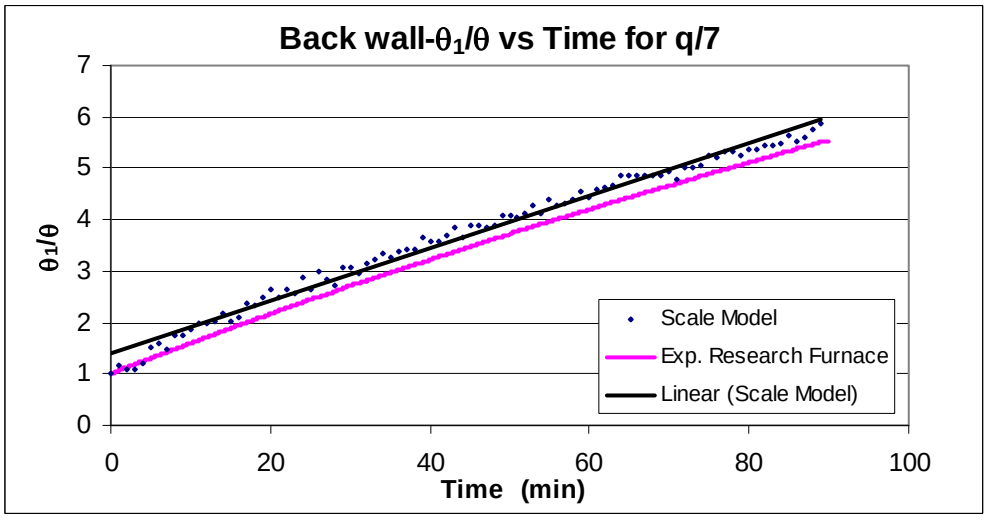

Figure 6.15 Temporal variation of θ_1/θ on the back wall of model furnace at q/7 heating intensity and compared with the data from the ERF furnace.

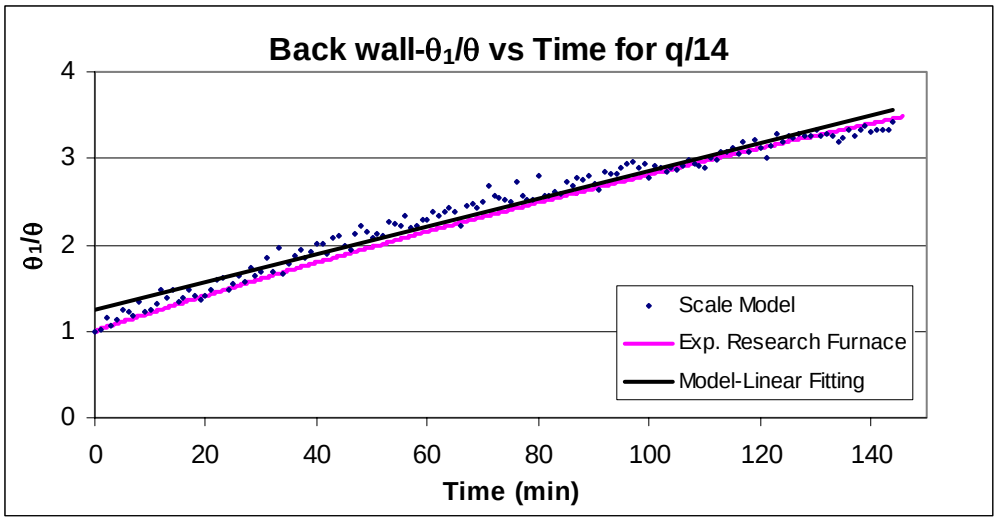

Figure 6.16 Temporal variation of θ_1/θ on the back wall of model furnace at q/14 heating intensity and compared with the data from the ERF furnace.

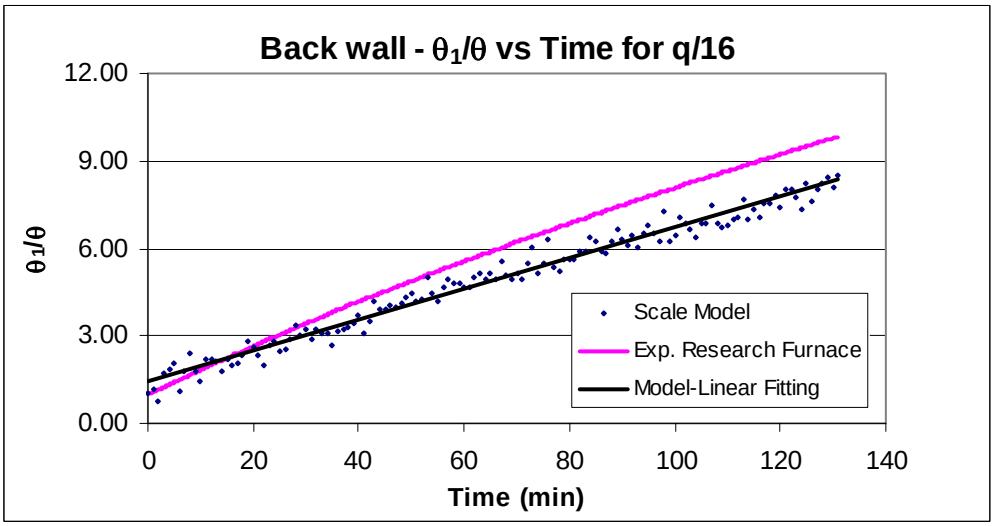

Figure 6.17 Temporal variation of θ_1/θ on the back wall of model furnace at q/16 heating intensity and compared with the data from the ERF furnace.

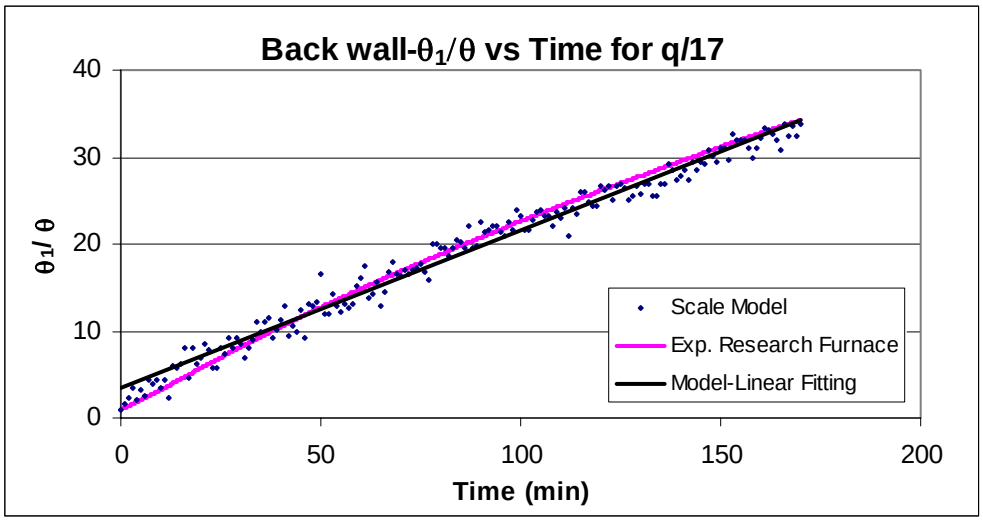

Figure 6.18 Temporal variation of θ_1/θ on the back wall of model furnace at q/17 heating intensity and compared with the data from the ERF furnace.

These plots show a good agreement of the data sets between these different sizes of the furnaces. Similar to the data shown in previous figures, a slight slope difference between the model tests and in the ERF furnace occur at the low heating intensity due to relatively longer heating period.

6.5 COMPARISON OF "θ1/θ" FOR ROOF

The temporal variation of θ_1/θ on the roof was tested and the results are shown in Fig. 6.19 for the heating intensity of q/4. Similar to the results shown in Fig. 6.13, the value of θ_1/θ is in good agreement with the tests for two different furnaces except the value of θ_1/θ on the roof is much larger than that on the back wall. This result is reasonable because thermal conduction across the furnace roof is much larger than that through the back wall.

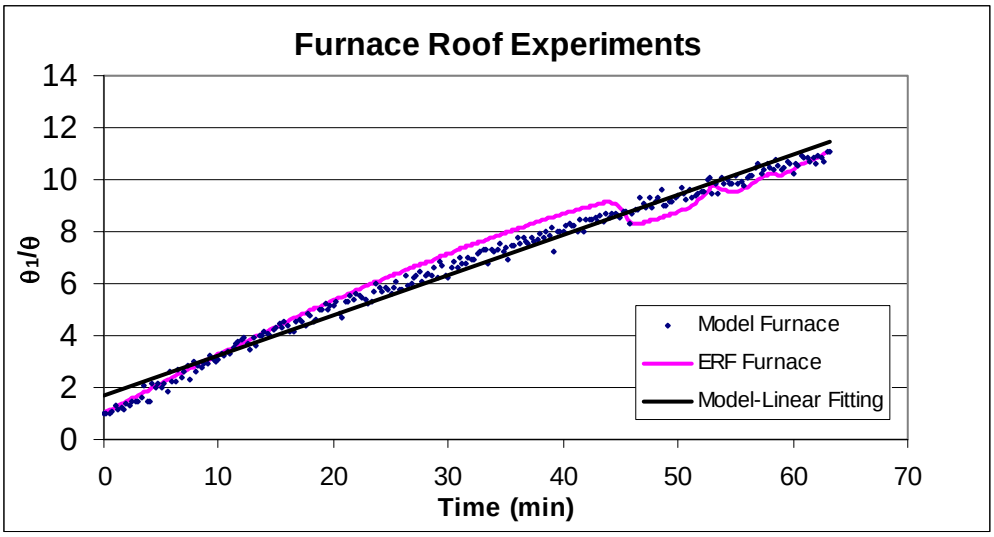

Figure 6.19 Temporal variation of θ_1/θ on the model furnace roof at q/4 heating intensity and compared with the data from the ERF furnace.

6.5.1 COMPARISON OF "θ_1/θ Vs. Time" FOR ROOF FOR SOME MORE CASES

More tests were conducted on the roof for θ_1/θ with the heating intensity at the values of q/5, q/7, q/14, q/16 and q/17 and the results are shown in figures 6.20-6.24.

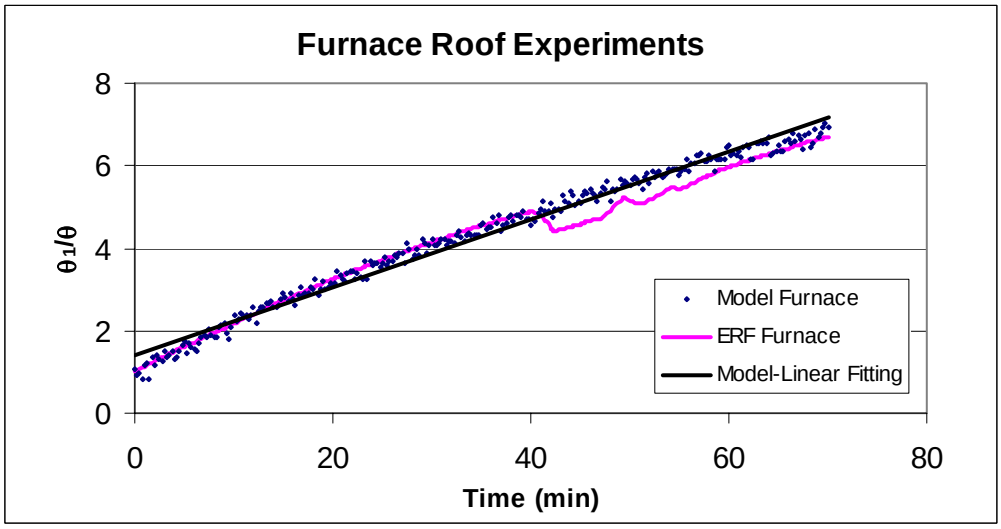

Figure 6.20 Temporal variation of θ_1/θ on the model furnace roof at q/5 heating intensity and compared with the data from the ERF furnace.

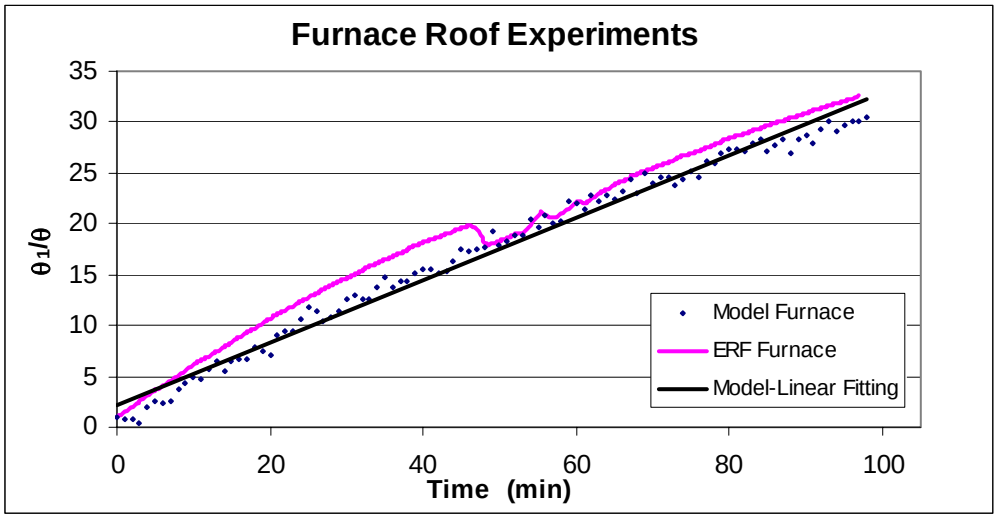

Figure 6.21 Temporal variation of θ_1/θ on the model furnace roof at q/7 heating intensity and compared with the data from the ERF furnace.

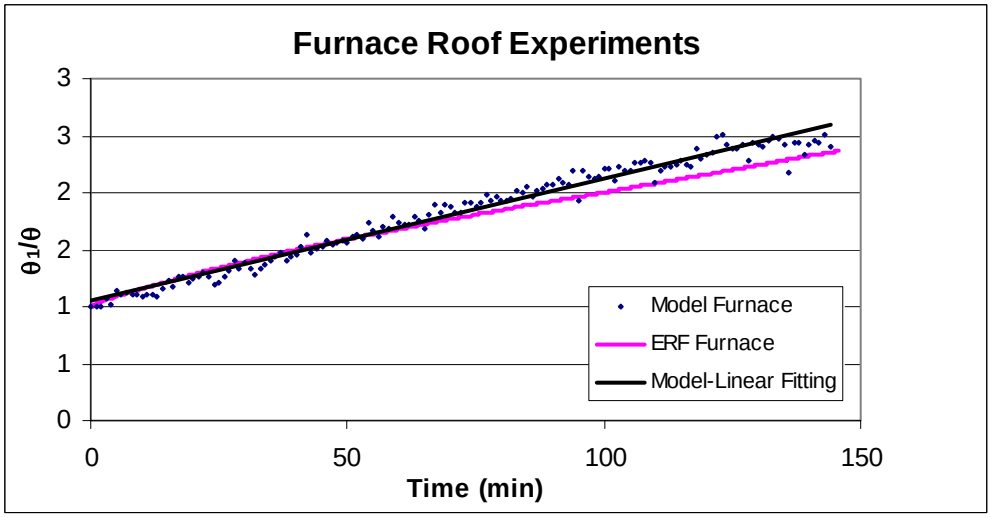

Figure 6.22 Temporal variation of θ_1/θ on the model furnace roof at q/14 heating intensity and compared with the data from the ERF furnace.

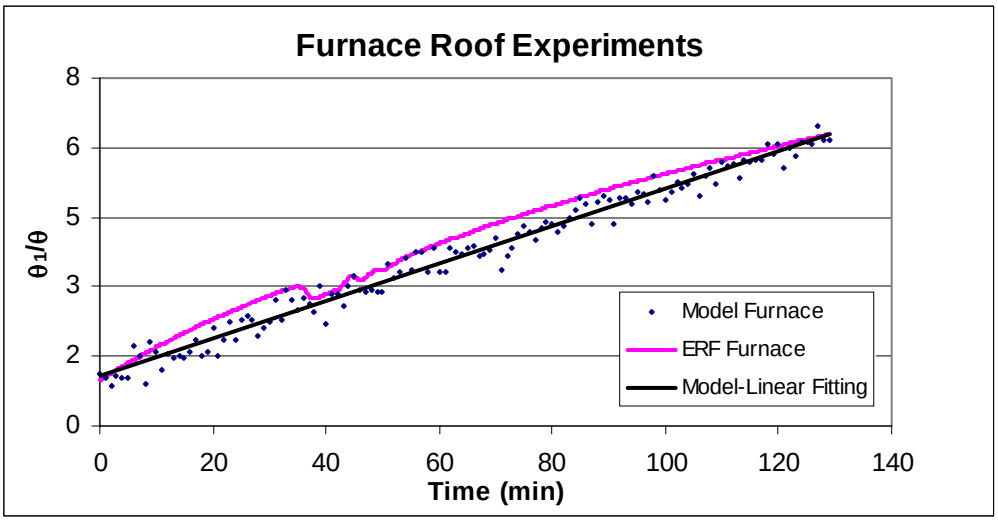

Figure 6.23 Temporal variation of θ_1/θ on the model furnace roof at q/16 heating intensity and compared with the data from the ERF furnace.

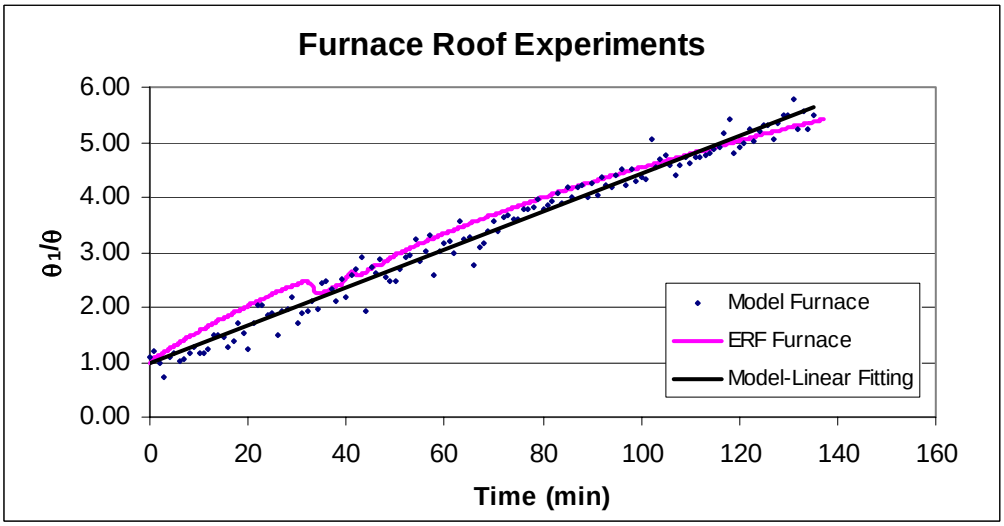

Figure 6.24 Temporal variation of θ_1/θ on the model furnace roof at q/17 heating intensity and compared with the data from the ERF furnace.

The good agreement when comparing the model experiments to the ERF tests verified that the group value of θ_1/θ is independent of the furnace size and may be valid without regard to the size.

6.6 EVALUATION OF COEFFICIENT OF HEAT TRANSFER BY CONVECTION (*h*) ON BACK WALL

According to our second pi number (Eq 4.6), the value of π_2 would be close to unity. This is based on the assumption that the thermal conduction loss through furnace walls would be carried away through heat convection at the wall boundaries. This implies that a negligible amount of heat gets stored in the furnace walls and the value of convective heat transfer quotient which could be obtained by balancing the two heat transfers should lie in the natural convection zone.

The experimental results for the values of *h* are presented in two groups according to the heating intensity. The first one includes the experiments results conducted at higher heat intensities of q/4, q/5 and q/7. The second one is the results obtained at lower heating intensities of q/16 and q/17. Figure 6.25 presents the values of coefficient of heat transfer by convection (*h*) across the back wall plotted against the time when the model furnace was run at higher heating intensities. The experiments were started at environmental temperature (20^0C) with no forced circulation in the room. These experimental conditions are similar to those for the tests in the ERF furnace.

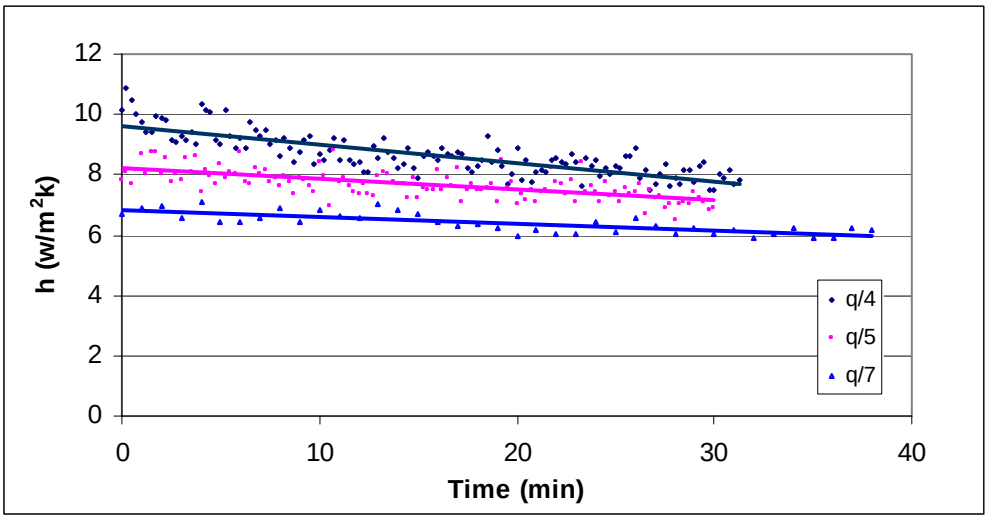

Fig 6.25 Temporal variation of Coefficient of heat transfer by convection (h) of back wall at higher heating intensities

Figure 6.25 demonstrates that the coefficient of heat transfer by convection in the model furnace back wall decreases with time, but increases with the heating intensity. The values of *h* on the back wall at high heating intensity are between 6 and 10 w/m^{2}k, and confirm that the convection is dominated by natural convection. The results confirm our statement that the value of π_2 is close to unity and that the heat conducted through the furnace would be carried away through heat convection at the wall boundaries. As natural convection is the phenomenon taking place in industrial furnaces as well as our prototype, the above results show that similar environmental conditions were applied on the scale model.

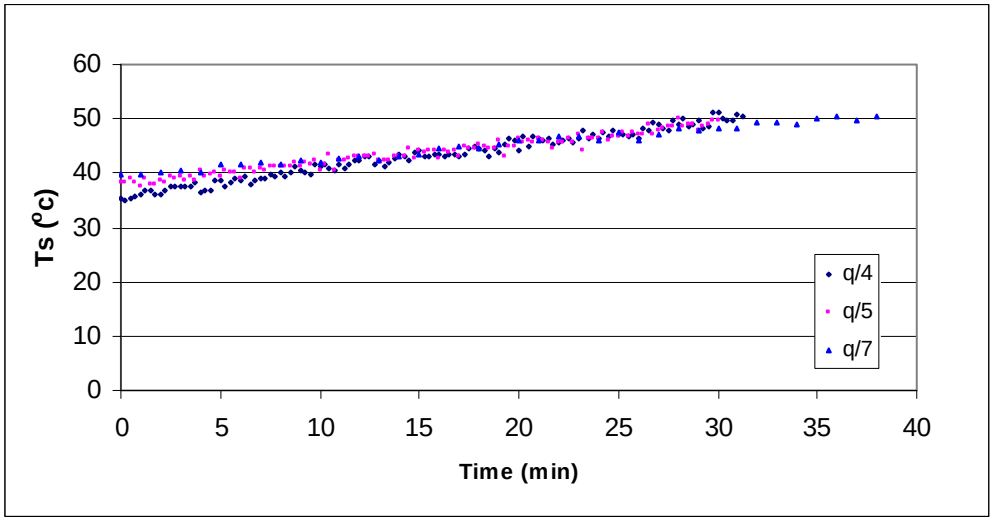

Fig 6.26 Temporal variation of the back wall surface temperature

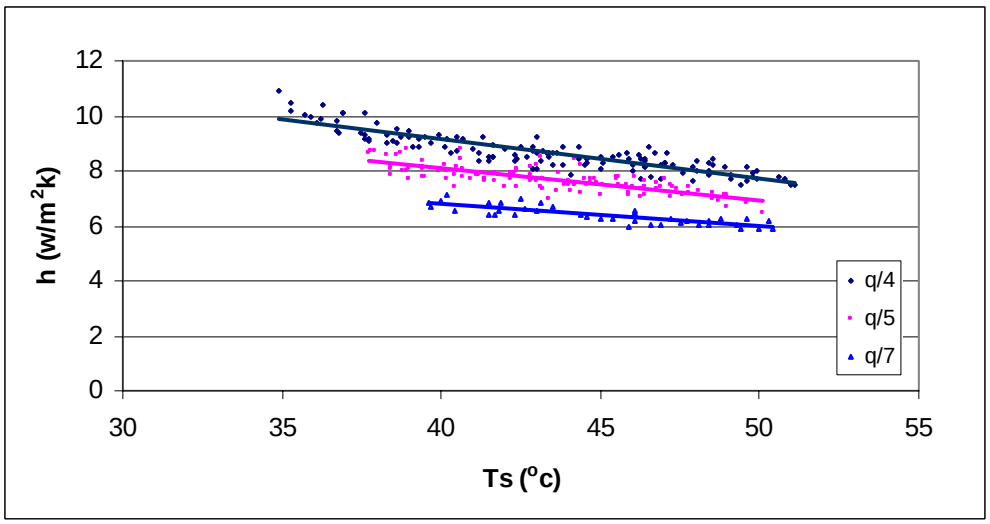

Fig 6.27 Variation of Coefficient of heat transfer by convection with wall surface temperature

Because the model experiments were conducted in an unsteady state, the wall surface temperature continuously increases. Figure 6.26 is the recorded exterior surface temperature of the back wall with time. It clearly shows that the exterior surface temperature of back wall increases from 35 °C to 50 °C in 40 minutes. The continuous increase of surface temperature on the back wall verifies transient nature of the furnace operation.

Thus, we can plot the change of *h* value with the wall surface temperature in Fig. 6.27. Figure 6.27 demonstrates that the values of the coefficient of heat transfer by convection decrease with the increase of wall surface temperature under current experimental conditions, and increase with the heating intensity in the model furnace. The higher the wall temperature, the higher is the value of the coefficient of heat transfer by convection.

6.6.1 COEFFICIENT OF HEAT TRANSFER BY CONVECTION (h) FOR BACK WALL FOR LOWER HEATING INTENSITIES.

Experiments were also conducted at lower heating intensities of q/16 and q/17 and the results are shown in Figs. 6.28 to 6.30.

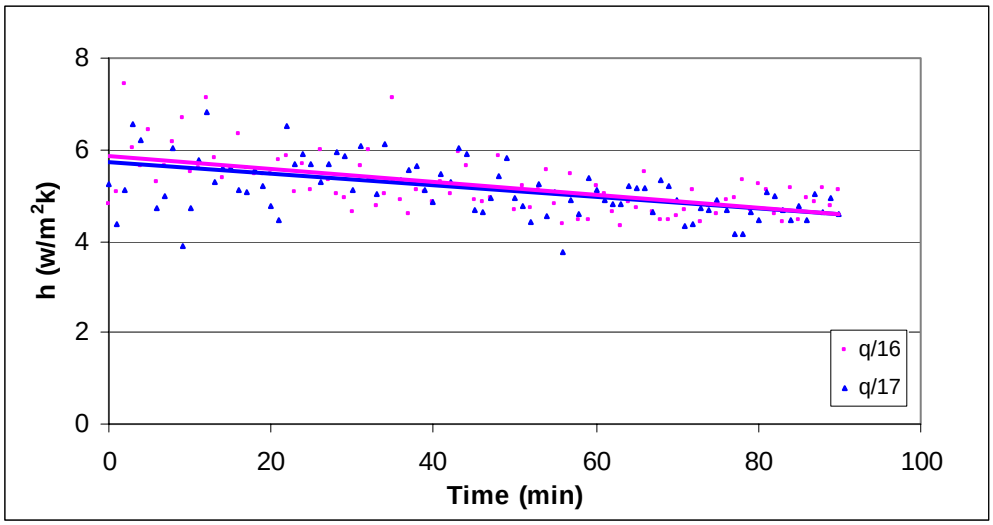

Fig 6.28 Temporal variation of Coefficient of heat transfer by convection (*h*) of back wall at lower heating intensities

Figure 6.28 shows a decreased variation of the values *h*, similar to those in Fig. 6.25. However, the values of *h* do not depend on the heating intensity, which is different from the case at high heating intensity. This phenomenon may be explained by the fact that the exterior surface temperature increases slowly at low heating intensity.

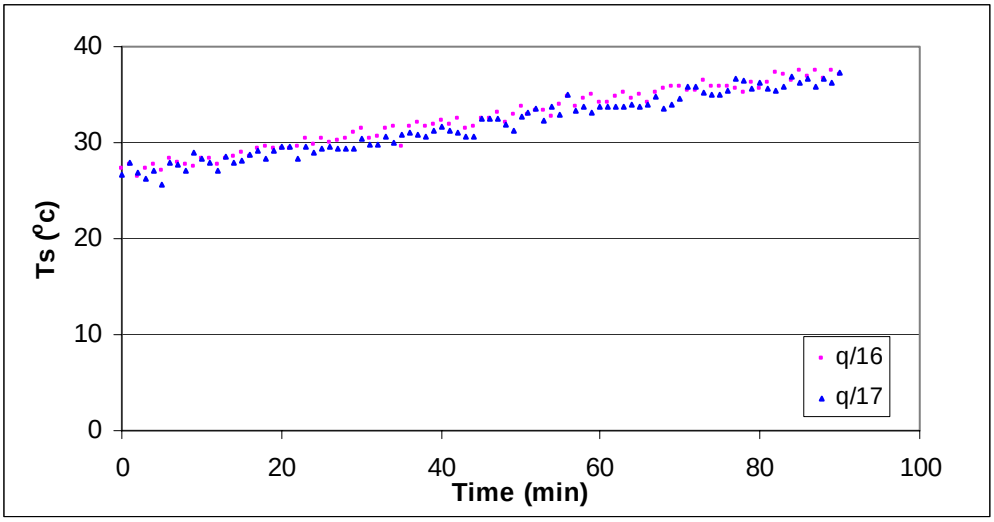

Fig 6.29 Temporal variation of back wall surface temperature

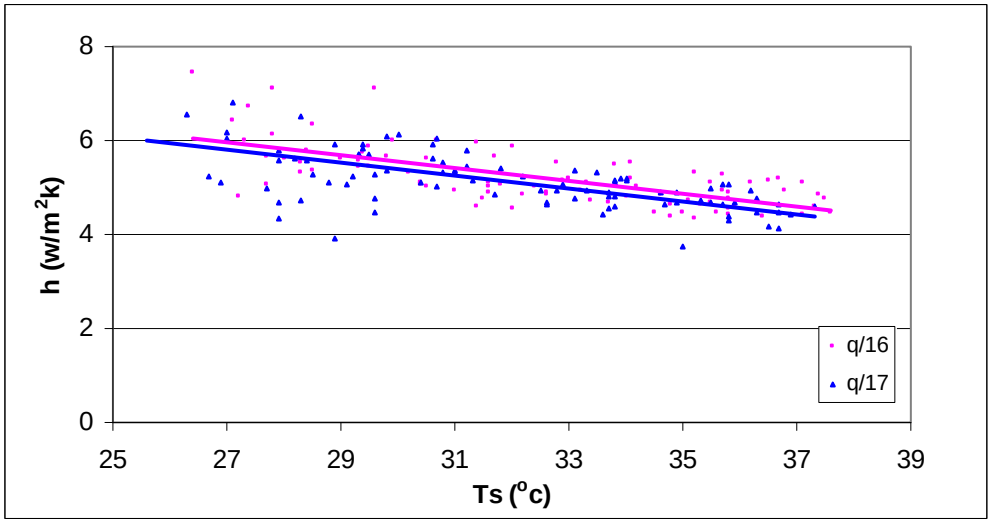

Fig 6.30 Variation of Coefficient of heat transfer by convection with back wall surface temperature

Figure 6.29 presents the temperature recorded for the back wall at low heating intensity. The exterior surface temperature increases from 25 °C to 38 °C in 90 minutes, much longer than those at high heating intensity. Therefore, we plot the value of *h* as a function of exterior surface temperature and the plot is shown in Fig. 6.30. It can be seen that the coefficient of heat transfer by convection *h* decreases as the temperature increases and is independent of the heating intensity in this case. The value of *h* is dominated by natural convection and is between 4 and 6 $w/m^2 \cdot k$, lower than those at high heating intensity.

6.7 EVALUATION OF COEFFICIENT OF HEAT TRANSFER BY CONVECTION (h) ON ROOF

As the heat transfer conditions for the roof are not entirely the same as those for the back wall, the coefficient of heat transfer by convection on roof was calculated separately. Same as the results shown for the back wall, we present the experimental results on back wall in two different groups - at high intensity and at low intensity.

Figure 6.31 shows the calculated value of coefficient of heat transfer by convection (*h*) across the roof plotted against the time when the model furnace was run at higher heating intensities of q/4, q/5, and q/7. The experiment was started from 20 ^{0}C room temperature with no forced circulation in the room.

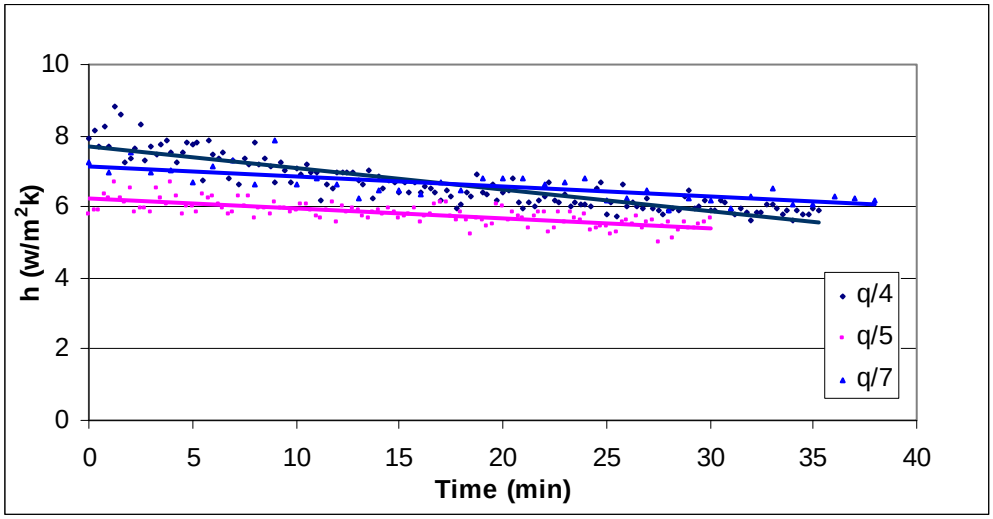

Fig 6.31 Temporal variation of Coefficient of heat transfer by convection (h) of roof at higher heating intensities

It can be seen in Fig. 6.31 that the value of heat transfer coefficient is decreased with time, and between 5 w/m^2·K and 9 w/m^2·K, in the region dominated by natural convection. It confirms our statement that the value of π_2 is close to unity and that the heat conducted through the furnace would be carried away through heat convection at the wall boundaries. As natural convection is the phenomenon taking place in industrial furnaces as well as the prototype, the results in Fig. 6.31 show that similar environmental conditions were applied on the scale model.

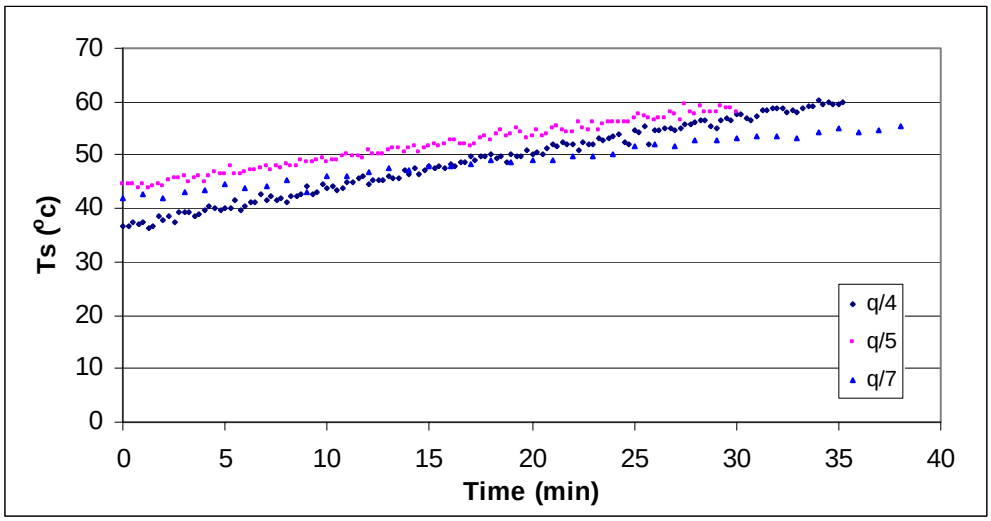

Fig 6.32 Temporal variation of Roof surface temperature (Ts)

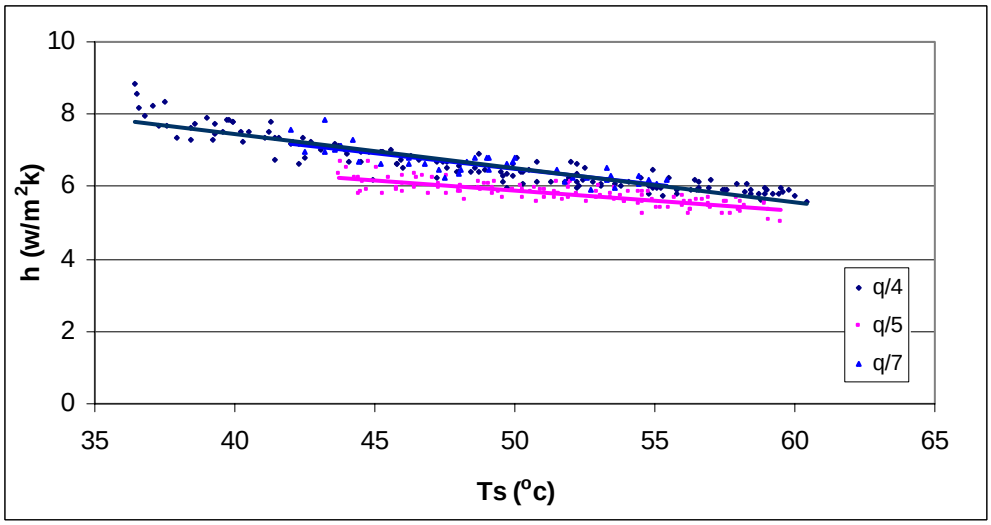

Fig 6.33 Variation of Coefficient of heat transfer by convection (h) of roof with surface temperature (Ts)

Figure 6.32 plots the exterior surface temperature of model furnace roof with experimental time. It shows an increased surface temperature, showing an unsteady state nature of the heating process. Thus, we can plot the coefficient of heat transfer by convection on the roof against the exterior surface temperature. This plot is shown in Fig. 6.33. It is demonstrated in Fig. 6.33 that the value of *h* decreases with the increase of temperature on roof exterior surface. The higher the roof temperature, the higher is the value of the coefficient of heat transfer by convection.

6.7.1 COEFFICIENT OF HEAT TRANSFER BY CONVECTION (h) FOR ROOF FOR LOWER HEAT INTENSITIES

The results of experimental values of *h* for the roof at low heating intensities of q/16 and q/17 are shown in Fig. 6.34 plotted against the experimental time. Similar to the results of *h*, at low heating intensity, the influence of heating intensity on the *h* is weak, and the two sets of data points at q/16 and q/17 heating intensity actually were merged. The value of *h* was slightly decreased because of lower heating intensity.

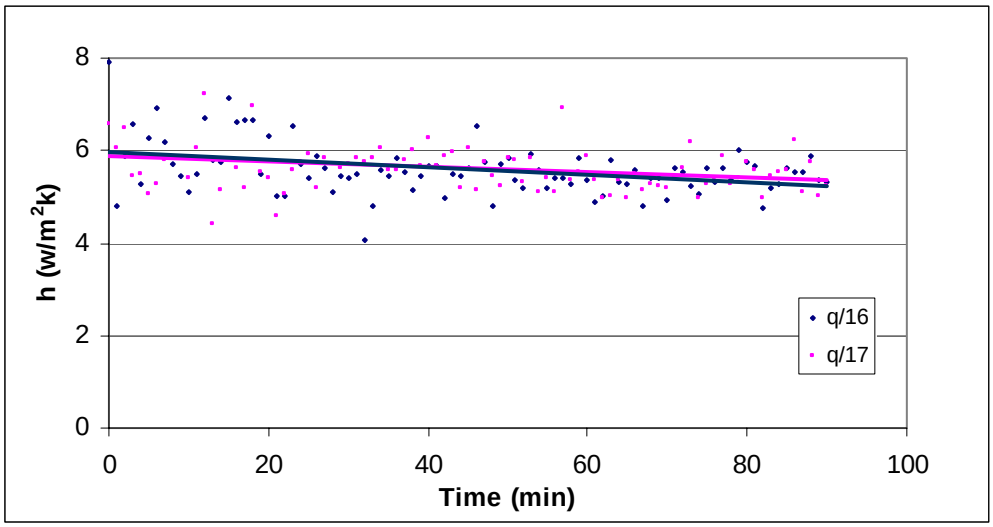

Fig 6.34 Temporal variation of Coefficient of heat transfer by convection (h) of roof at lower heating intensities

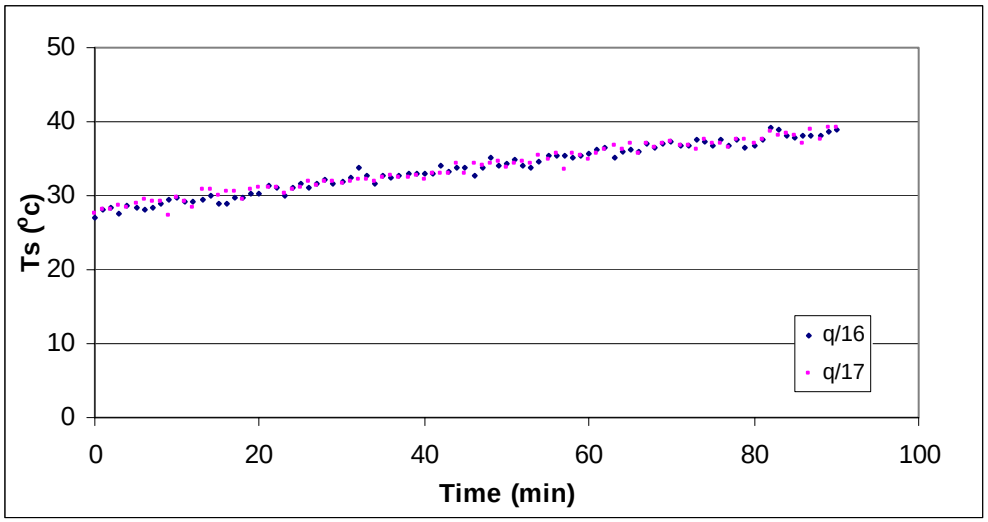

Fig 6.35 Temporal variation of roof surface temperature at lower heating intensities

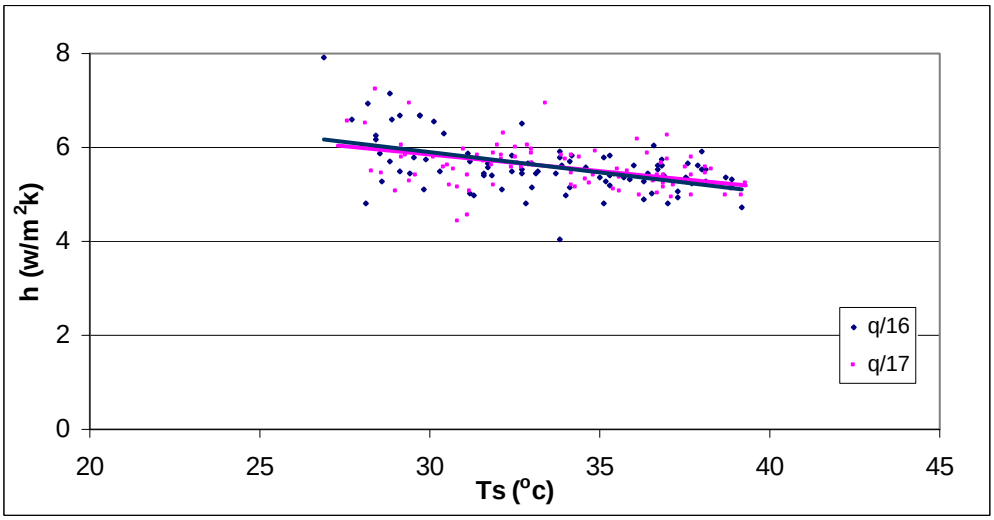

Fig 6.36 Variation of Coefficient of heat transfer by convection with wall surface temperature

The exterior surface temperature of the roof at low heating intensity in Fig 6.35 shows an increase tendency. Thus, the coefficient of heat transfer by convection at low heating intensity can be plotted as a function of exterior surface temperature, and is presented in Fig. 6.36. It can be seen that the trend of *h* on roof is similar to its behavior at higher heat intensities, except the effect of heating intensity on the value of *h* in this case is weak. The results for the roof are similar to the observations on the back wall of the model furnace.

CHAPTER 7
CONCLUSION

In this thesis, the appropriate scaling laws were developed and applied to the aluminum furnace by following the partial scaling technique. A new model experimental furnace was designed and cast, whose dimensions are 1/4th of that of the ERF furnace at the Albany Research Center of the U.S. Department of Energy, which has been considered as the prototype in this study. The materials used in the model furnace are the same as those used in the ERF furnace. A series of tests on the thermal conduction loss across the back wall and roof were separately conducted in the model furnace and the ERF furnace, and a comparison was made for the results obtained from these two different furnaces. The ERF furnace was directly fired with natural gas, the aluminum load was melted and the melting processes are very similar to those in the industrial furnaces. While in the model furnace, the tests were conducted using electrical heaters and the aluminum load was used only for absorption of heat instead of melting. This is because the model furnace was operated at lower temperatures than the ERF furnace because of thinner furnace walls. The measurements on the model furnace were limited to the thermal conduction loss along the back walls and roof.

Although the test processes in these two furnaces are quite different, the processes in the model furnace are not really melting; comparisons of thermal conduction loss between these two furnaces show a good agreement. The experimental results show that the group values of θ_1/q and θ_1/θ obtained from the model furnace are only a function of time, and independent of the furnace size. At low heating intensity, there exists a slight difference in slopes of θ_1/q and θ_1/θ between two separate tests due to longer heating time in the model experiments. The value of coefficient of heat transfer by convection was determined in the model experiments. The results show that the heat convection in the model experiments was dominated by natural convection.

The good agreement in comparison of the values, θ_1/q and θ_1/θ, and their nature of being independent of the furnace dimensions, imply that these two groups may be transferred to the other furnaces without size considerations. The experimental results show that scale modeling is a valuable tool applied to the aluminum furnace, one which can help to validate the test results performed on a small scale furnace to the prototype as long as the scaling laws are followed. More experiments may be needed on melting processes to test the validity of other parameters.

APPENDIX

NOMENCLATURE

Dimensional Symbols

C_p	specific heat *(j/g K)*
d	wall thickness *(m)*
h	coefficient of heat transfer by convection *(W/m^2K)*
k	thermal conductivity *(W/m K)*
l	characteristic length *(m)*
q^*	heating intensity *(W/m^3)*
Q_c	total heat loss by convection *(j)*
Q_g	heat generation *(j)*
Q_k	heat conduction in time t *(j)*
Q_s	heat storage in time t *(j)*
t	time *(s)*
ΔT_1	temperature gradient along the wall *(K)*
$\Delta T2$	temperature difference in wall boundary and ambient *(K)*
T_3	average temperature across the wall *(K)*
θ_1	temperature in representative form in heat conduction *(K)*
θ_2	temperature in representative form in heat convection *(K)*
ρ	density *(kg/m^3)*

Dimensionless Symbols

Bi	Biot number, ratio of heat convection to heat conduction within solid body
$Da_{,IV}$	(4^{th}) Damköhler number, ratio of heat conduction to heat generation
Fo	Fourier number, ratio of heat conduction to heat capacity
α	thermal diffusivity

REFERENCES

1. Choate, W.T., Green J.A.S., U.S. Energy Requirements for Aluminum Production: Historical Perspective, Theoretical Limit and New Opportunities, U.S. Department of Energy, Energy Efficiency and Renewable Energy, Washington, D.C., (2003).
2. Nancy Margolis, Energy and Environmental Profile of the U.S. Aluminum Industry, U.S. Department of Energy, Office of Industrial Technologies, (1997).
3. Tianxiang Li, Mohamed Hassan, Kazunori Kuwana, Kozo Saito, Srinath Viswanathan, Qingyou Han and Paul King. Thermodynamic Analyses of Energy Utilization and Pollutant Formation Control in Secondary Aluminum Melting Furnaces, Energy Efficient Manufacturing Processes, The Materials Processing and Manufacturing Division of TMS, pp. 43-51, The 132nd TMS Annual & Exhibition, San Diego, CA, March 2-6 (2003).
4. Johnstone and Thring, Pilot Plants, Models, and Scale-up Methods in Chemical Engineering, McGraw (1957).
5. Dieterich J Schuring, Scale Models in Engineering-Fundamentals and Applications, Calspan Corporation, Buffalo, New York (1997).
6. Hirano, H. and Saito, K., Fire Spread Phenomena: The Role of Observation in Experiment, Prog., Energy Combust. Sci., Vol. 20 pp. 461-485, (1994).
7. Emori, R. I., K. Saito, and K. Sehimoto, Mokei Jikken No Riron To Ohyou, 3rd Edition, Gihodo Pub., 2000 (in Japanese).
8. Sita rama raju S. Penmetsa, Tianxiang Li, and Kozo Saito, Scaling Aluminum Melting Furnaces, Proceedings of 4th International Symposium on Scale Modeling, pp. 317-324, Cleveland, OH, Sep. 17-19, (2003).

VITA

Date and Place of Birth

- August 15, 1979 at Bhimavaram, Andhra Pradesh, India

Education

- Bachelor's degree in Mechanical Engineering (B.Tech), VNRVJ Institute of Engineering and Technology, affiliated to Jawaharlal Nehru Technological University, Hyderabad, India (2001)

Work Experience

- Worked as Research Assistant at the University of Kentucky, Department of Mechanical Engineering. (June 2002- December 2003)

Technical Publications

- Sita rama raju S. Penmetsa, Tianxiang Li, and Kozo Saito, Scaling Aluminum Melting Furnaces, Proceedings of 4th International Symposium on Scale Modeling, pp. 317-324, Cleveland, OH, Sep. 17-19, (2003).
- Sita rama raju S. Penmetsa, Tianxiang Li, Paul King and Kozo Saito, Scale Modeling of Aluminum Melting Furnaces, Light Metals 2005, Edited by Halvor Kvande, TMS (The Minerals, Metals & Materials Society) 2005, San Francisco, CA, Feb 2005.